Age-dependent Lamin remodeling induces cardiac dysfunction via dysregulation of cardiac transcriptional programs

Natalie Kirkland
University of California, San Diego
Alexander Whitehead
University of California, San Diego
James Hocker
University of California, San Diego
Pranjali Beri
University of California, San Diego
Geo Vogler
Sanford Burnham Prebsy Medical Discovery Institute
Bill Hum
Sanford Burnham Prebsy Medical Discovery Institute
Mingyi Wang
National Institute on Aging https://orcid.org/0000-0001-6412-369X
Edward Lakatta
National Institute on Aging
Bing Ren
University of California, San Diego
Rolf Bodmer
Sanford Burnham Prebys Medical Discovery Institute
Adam Engler (aengler@ucsd.edu)
University of California, San Diego https://orcid.org/0000-0003-1642-5380

Article

Keywords: Sarcomere, transcription factor, nuclear lamina, lifespan, nuclear stiffness, chromatin accessibility

Posted Date: November 11th, 2021

DOI: https://doi.org/10.21203/rs.3.rs-1021378/v1

Age-dependent Lamin remodeling induces cardiac dysfunction via dysregulation of cardiac transcriptional programs

(Author names redacted)

MANUSCRIPT INFORMATION

Abstract Count: 150 words

Main Text Character Count: 41,264 (including spaces and figure legends but excluding Methods text, supplemental item legends, and References section)

Figure Count: 7

Supplemental Figure Count: 6

Supplemental Table Count: 10

Keywords: Sarcomere, transcription factor, nuclear lamina, lifespan, nuclear stiffness, chromatin accessibility

RUNNING TITLE

Age-associated Nuclear Remodeling Drives Cardiac Dysfunction

Abstract

As we age, structural changes contribute to progressive decline in organ function, which in the heart acts through poorly characterized mechanisms. Utilizing the rapidly aging fruit fly model with its significant homology to the human cardiac proteome, we found that cardiomyocytes exhibit progressive loss of Lamin C (mammalian Lamin A/C homologue) with age. Unlike other tissues and laminopathies, we observe decreasing nuclear size, while nuclear stiffness increases. Premature genetic reduction of Lamin C phenocopies aging's effects on the nucleus, and subsequently decreases heart contractility and sarcomere organization. Surprisingly, Lamin C reduction downregulates myogenic transcription factors and cytoskeletal regulators, possibly via reduced chromatin accessibility. Subsequently, we find an adult-specific role for cardiac transcription factors and show that maintenance of Lamin C sustains their expression and prevents age-dependent cardiac decline. Our findings are conserved in aged non-human primates and mice, demonstrating age-dependent nuclear remodeling is a major mechanism contributing to cardiac dysfunction.

Introduction

With aging comes a progressive decline in organ function[1,2], but age-related decline in heart performance is especially critical as cardiovascular disease is the leading cause of mortality worldwide[3]. Aging results in the progressive loss of structural organization[4,5], which can limit contractility[1,6] and result in heart failure[7]. High prevalence of age-related cardiac dysfunction may in part be because cardiomyocyte renewal is limited[8] and therefore, maintenance of cardiac function over time must rely on compensatory mechanisms; these are multifaceted but tightly linked to the integrity of key structural elements, e.g., intercalated discs, sarcomeres, and extracellular matrix. Reducing force on cardiomyocytes (CMs) or compensating with transgenic overexpression of intercalated disc proteins can partially reverse heart dysfunction, typically by restoring structural organization and gene expression[6,7]. Since physical forces transduced to the nucleus can impact chromatin organization and induce changes in gene expression[9–11], nuclear remodeling may similarly be a mechanism of age-associated cardiac dysfunction.

Structural changes in the nucleus are primarily governed by the nuclear lamina, an intermediate filament meshwork composed of A- and B-type Lamins. The lamina is tethered to the

cytoskeleton[12,13] via the linker of the cytoskeleton (LINC) complex[9–11] as well as to chromatin[14,15] via lamina associated domains (LADs)[16]. Along with the perinuclear cytoskeleton[12,13] and chromatin[14,15], the nuclear lamina regulates nuclear properties, including stiffness, size and shape[17–26]. In mechanically active tissues, Lamin mutations give rise to muscular dystrophy[27,28] and cardiomyopathies[29], which also manifest in premature aging syndromes, e.g., Hutchinson Gilford Progeria (HGPS)[30]. Lamin mutations cause dysmorphic nuclei, epigenetic dysregulation and DNA damage[31–34]. However, changes in nuclear shape, which are conserved from invertebrates[35,36] to humans[37], have been observed upon aging in the absence of Lamin mutations and accompany loss of heterochromatin[37,38] and accumulation of DNA damage[37]. In some cases, Progerin (truncated Lamin A) has been identified in aging skin[39] and dilated cardiomyopathy[40] in the absence of mutations. Furthermore, Lamins decrease in expression with age in some tissues[41–43], with loss of Lamin B being a well-known aging marker[42] that may decrease cardiomyocyte regenerative capacity and increase ploidy[44]. Lamin A and C (Lamin A/C, two splice variants of the *lmna* gene) are the dominant adult cardiac Lamins, and age-associated reduction has been observed in mouse cardiomyocytes[41], but a role in heart function and cardiac aging is unknown. Insights from Lamin A haploinsufficient mutant mice suggest Lamin reduction is as detrimental to heart function as progerin mutants; mice develop dilated cardiomyopathy via loss of sarcomere-nuclear coupling, show defective nuclear transport and fail to activate compensatory hypertrophic pathways[45]. Thus, age-associated nuclear remodeling could be a major mechanism contributing to organ dysfunction, yet mechanisms contributing to age-dependent nuclear remodeling and how it affects tissue function remain elusive.

To investigate a role for age-dependent nuclear remodeling in regulating heart function, we primarily employ the invertebrate *Drosophila melanogaster*. *Drosophila* are rapidly aging, possess a simple but highly conserved heart[46], and importantly, demonstrate age-depended cardiac decline[5,47]. We identified age-dependent remodeling unique to CM nuclei, which is strongly influenced by an age-dependent reduction of Lamin C (LamC), the fly homologue to mammalian Lamin A/C. Genetic reduction of LamC in young flies phenocopies age-associated nuclear stiffening, decreased heart contractility and sarcomere disorganization, and ultimately shortens lifespan. We show that LamC loss decreases expression of cardiomyocyte transcription factors, as well as cytoskeletal regulators, likely by reducing their chromatin accessibility.

Premature reduction of CM transcription factors partially phenocopies age-dependent loss of heart function, while reinstating LamC levels in adult flies prevents transcription factor loss and improves heart function. CM age-associated nuclear shrinkage is conserved from flies to non-human primates and therefore presents nuclear remodeling as a major mechanism contributing to age-related organ dysfunction.

Results

Cardiomyocyte nuclei remodel during aging

To understand whether age-associated nuclear remodeling influences heart function, we first sought to characterize how nuclear properties change upon aging in the *Drosophila* heart. Using two wildtype strains (w^{1118} and *yw*), we measured nuclear size and shape at 1, 3 and 5 weeks post-eclosure for surgically exposed hearts and specifically the A2-A3 region (Fig. 1A). Our high-throughput two-dimensional segmentation approach showed that common to both strains, CM nuclei decrease in cross-sectional area and became more circular upon aging (Fig. 1B and S1A-C), which is contrary to long-standing observations in other cell types, e.g., skeletal muscle nuclei[36] and fibroblasts[37]. To exclude that our observations were an artifact of our protocol, we segmented nuclei from the syncytial ventral muscle that overlays the CM pairs within the same confocal images (Fig. 1A). Here, we found that ventral muscle nuclei increase in size upon aging, suggesting the reduction in nuclear size is CM specific (Fig. S1D). Nuclear atrophy is conserved in three-dimensions, as we found that CM nuclear volume also decreases with age in w^{1118} flies (Fig. 1C and S1E). Since morphology and mechanics are often linked, we measured nuclear stiffness at 1 and 5 weeks of age using atomic force microscopy (AFM). CM nuclei, selected based on *Hand*-promoter specific nuclear GFP expression and size (smaller than the pericardial nuclei), were more than 2-fold stiffer in aged flies (Fig. 1D). Together, our results show that CM nuclei become smaller, more circular, and stiffer with age.

Lamin RNA and protein levels decrease in cardiomyocytes during aging

To identify candidate genes that may regulate age-associated nuclear remodeling, we performed bulk RNA sequencing on isolated *Drosophila* heart tubes to identify candidate genes that may regulate age-associated nuclear remodeling (Fig. 2A; Table S1). Approximately 1,487 differentially expressed genes (DEGs; $-1.25 > FC > 1.25$, p-adj < 0.05) were identified and based

on gene ontology (GO) analysis represented terms primarily related to the cytoskeleton and sarcomere, ECM and adhesion, and chromatin regulation and nuclear envelope (Fig. 2B; Table S2). Many DEGs in this latter ontology (Fig. S2A) are common to age-related terms, e.g., DNA damage, repair, and histone regulation (Fig. S2B). Interestingly, several nuclear envelope genes were downregulated including Lamin C (LamC) and two homologues of Nesprin, LINC complex proteins, Klarischt (Klar) and Msp300 (Fig. 2C). Utilizing *in situ* Hybridization Chain Reaction (HCR)[50] to visualize mRNA transcripts and confirm transcriptome analyses specifically in CMs, we found that LamC mRNA expression indeed decreases upon aging as did Lamin B (LamB) transcripts (Fig. S2C-D) consistent with other aging systems[51]. Other cell types present in the heart may explain the absence of differential expression for LamB in bulk RNA sequencing (Fig. 1A). Subsequently, we verified via corrected total nuclear fluorescence (CTNF) that size-normalized expression of LamB and LamC decreased upon aging (Fig. 2D and S2E). However, unlike in Progeria and aged donor fibroblasts where Lamin A/C relocates from nucleoplasm to nuclear envelope[37], Lamins did not show a redistribution within aged nuclei (Fig. S2E).

Cardiomyocyte Lamin C reduction phenocopies age-related nuclear and cytoskeletal remodeling, and shortens lifespan

Strong evidence from patients with laminopathies[23,37] suggest that Lamins regulate cell function and contribute to heart dysfunction[49]. However, evidence does not suggest what effects, if any, there might be in aged hearts. To determine the effect of age-associated Lamin downregulation on CM function, we employed and verified cardiac-targeted RNAi for LamB and LamC through development relative to their background controls (*attp40* for *LamB RNAi* and *attp2* with Luciferase control RNAi for *LamC RNAi*; Fig. 3A and S3A-B). Using the non-targeted Lamin to mark nuclear lamina, we observed that LamC and LamB reduction decreased nuclear area and perimeter but only *LamB RNAi* increased circularity at 1 week of age (Fig. 3B and S3C). However, the effect size was age-dependent because controls undergoing age-associated remodeling more closely mirrored RNAi effects after 4 weeks of adulthood (Fig. S3D). These distinct effects on nuclear morphology indicate that LamC and LamB may dissimilarly influence nuclear properties. Indeed, nuclei extracted from *LamC RNAi* hearts at 1 week were stiffer than age-matched controls and mimicked aged controls, while *LamB RNAi* hearts were softer than controls and did not phenocopy aging (Fig. 3C).

Along with nuclear stiffness, we found differential effects on heart function upon LamB or LamC reduction. Surgically exposed hearts from 1 week and 4 week-old adults were subjected to live, high-speed imaging[52]. We observed that *LamC RNAi* hearts decreased in fractional shortening, i.e., the difference of systolic and diastolic heart diameters divided by the diastolic diameter, relative to age-matched controls (Fig. S3E-F). Conversely, *LamB RNAi* hearts only exhibited age-associated diminished contractility (Fig. 3D-E). Since hearts with reduced LamC were less contractile, we examined how organized the sarcomeres, i.e., the contractile unit of CMs, were to assess whether organization might account for reduced fractional shortening. Using an automated, unbiased Fourier transform analytic[53], we found a significant decrease in sarcomere organization for *LamC RNAi* hearts relative to age-matched controls, which phenocopies 4-week adult heart organization. Consistent with functional data, *LamB RNAi* hearts only exhibited age-associated diminished organization (Fig. 3F-G). As heart function is tightly linked to survival in *Drosophila,* we observed that only *LamC RNAi* flies had a shortened lifespan (Fig. 3H). These results suggest that LamC loss during aging contributes to heart dysfunction via sarcomere disorganization.

Aging and Lamin C reduction lead to changes in chromatin accessibility and influence mesoderm transcription factor loci

While heart dysfunction may occur via sarcomere disorganization, conserved upstream mechanisms for *LamC RNAi* and natural aging are unknown. Given Lamins' role in anchoring chromatin and their link to cardiomyopathies[54], we hypothesized that cardiac dysfunction induced by Lamin deficits are mediated by changes in age-associated chromatin organization**.** Assay for Transposase-Accessible Chromatin sequencing (ATAC-Seq) was performed on isolated heart nuclei, and we verified detection of accessibility peaks mapping to *Drosophila* heart-specific and enriched genes *Hand* and *tinman (tin)* and sarcomere genes *Tropomyosin* and *Mhc* (Fig. 4A). Subsequently, we compared differentially accessible regions (DARs) for 1- and 5-week wildtype (w^{1118}), *LamC RNAi* and *LamB RNAi* hearts (-1.25 > FC > 1.25, p-adj < 0.1). There were more DARs with aging compared to RNAi hearts (Fig. 4B; Table S3), likely because aging impacts all cardiac-related cells whereas the RNAi was expressed only in CMs, which are a subset of all cells present in the heart tube (Fig. 1A). Surprisingly with less LamC, hearts had more DARs that were less accessible vs. more accessible, an imbalance also

observed in aging hearts (67.5% and 55.9%, respectively). Conversely, *LamB RNAi* had fewer DARs overall and fewer that were less accessible (38.0%). Thus, while nuclei get smaller and stiffer in aged and *LamC RNAi* hearts, there are also changes in chromatin accessibilty.

These data could suggest that *LamC* reduction might have effects on specific chromatin domains during aging, thus we asked to what extent the same genes were affected in the same direction for both aging and *LamC RNAi*. Analysis of DARs common to both datasets indicated that 68% of DARs were co-regulated, with more than half being less accessible (Fig. 4C; Table S4). Conversely, more DARs shared between *LamB RNAi* and aging were mutually more accessible. These results indicate that *LamC* and *LamB* may differentially contribute to changes observed during aging, with *LamC* reduction conferring a decrease in accessibility associated with a decline in heart performance.

To better understand how co-regulated DARs might contribute to loss of function, we identified the ontological terms associated with the less accessible regions. Mutually less accessible genes revealed terms for contractile fibers and cell cortex in addition to differentiation, development, and morphogenesis (Fig. 4D; Table S5). Interestingly, the most highly significant terms' contributing genes included the Snail-type transcription factor Escargot and the heart-specific transcription factor Hand (Fig. 4E), which do not change in accessibility for *LamB RNAi* (Fig. 4F). Hand is required for invertebrate and vertebrate CM specification[55], and therefore may function beyond development to maintain cardiac programs. If reduced chromatin accessibility leads to protein loss upon aging, it is possible that downstream cardiac expression could be dysregulated.

Cardiomyocyte Lamin C loss exhibits a premature aging expression profile and decreases cardiomyocyte transcription factors

To assess whether altered chromatin accessibility might lead to transcriptional dysregulation, and if other cardiac specific transcription factors were affected, we performed bulk-RNA sequencing for aged and *LamC RNAi* hearts. We observed 344 differentially expressed genes (DEGs) with heart-specific *LamC* loss and 1,998 DEGs in aged *attp2* background flies ($-1.25 > FC > 1.25$, padj < 0.05; Fig. 5A, Table S6-7) from which 688 DEGs were co-regulated in the original w^{1118} control aged hearts (Fig. S4A-C; Table S8). We then identified mutually significant DEGs from *LamC RNAi* and aged hearts and observed that 111 DEGs were conserved in both

conditions (Fig. 5B; Table S9). Mutually conserved genes presented biological process terms related to aging (red, Fig. 5C; Table S9), suggesting that LamC loss creates differential gene expression similar to natural aging. As validation, we also observed terms previously identified from ATAC-Seq, including anatomical structure development and morphogenesis (blue, Fig. 5C), in which CM transcription factors *tin* and *H15* were downregulated (Fig. 5D). HCR validated CM specificity of *tin*, *H15,* and *Hand* and showed that all three were reduced in both aged and *LamC RNAi* hearts (Fig. 5E). Conversely for *LamB RNAi*, hearts showed only an aging phenotype and no transgenic effect (Fig. 5E and S4D-E). Our results thus far show that *LamC* loss occurs with age, makes nuclei smaller and stiffer, decreases CM transcription factor accessibility and expression and then disrupts sarcomeres to cause contractile dysfunction. However, our results do not yet establish if loss of a myogenic program is critical for adult myocyte function.

Adult-onset myogenic transcription factor loss induces heart dysfunction while LamC preserves heart function

The importance of myogenic transcription factors is highlighted by significant sarcomere defects present when any one factor is silenced throughout development (Fig. S5A). This begs the question of whether CM transcription factor loss in adulthood, due to age-associated LamC loss, could influence heart function. To reduce expression only in the adult fly and assess whether their loss phenocopies LamC reduction, flies possessing the temperature sensitive suppressor of Gal4, *TubGal80^{ts},* and heart specific drive Hand-Gal4 were used (Fig. 6A). Within 24 hours of eclosure, adult flies were maintained at the permissive (18^{o}C) or shifted to the non-permissive temperature (29^{o}C), and after 2 weeks their heart function assessed. Live heart imaging showed that loss of each transcription factor only in adulthood still caused a significant decrease in fractional shortening compared to control backgrounds which exhibit a slight, but insignificant reduction in fractional shortening due to relative differences in aging between flies maintained at 18^{o}C verses 29^{o}C (Fig. 6B-C and S5B).

Conversely, we asked if adult-onset *LamC* overexpression could preserve myogenic factor expression and function with age. When LamC expression is induced at 29^{o}C, we observed nuclear size was consistent with 18^{o}C flies, in contrast to GFP overexpression controls that showed an expected age-dependent reduction in nuclear size (Fig. 6D and S5C). LamC protein levels did not significantly decrease, in contrast to GFP overexpression controls (Fig.

S5D), which corresponded to an increase in LamC transcript levels only at 29ºC for LamC OE hearts (Fig. S5E). Importantly, with additional *LamC* in older flies, fractional shortening was preserved (Fig. 6E and S5F), as well as CM specific expression of myogenic transcript factors *tin*, *H15,* and *Hand* (Fig. 6F-G). Together, our results establish that adult loss of myogenic programs is mediated by age-associated *LamC* loss and their chromatin remodeling, which subsequently reduces adult cardiomyocyte function (Fig. 7A).

Nuclear Remodeling and Adult-onset Transcription Factor Loss is Conserved in Mice and Non-human Primates

Despite physiological differences between tubular and chambered hearts, there is surprising overlap between the *Drosophila* and human cardiac proteomes[46]. We therefore sought to assess whether similar structural and transcriptional changes are conserved from the fly heart to the mammalian heart[41]. We observed in both mouse and monkey heart sections that nuclear size decreased and circularity increased upon aging, as we found in the fly heart tube (Fig. 7B-C). Furthermore, immunofluorescence staining of the mouse heart sections confirmed reduction of Lamin A/C (Fig. 7B), consistent with *Drosophila*. Subsequently, we found mammalian homologues of fly transcription factors, *Hand1, Nkx2*.5 (homologue of *tin*), and *Tbx20* (homologue of *H15*) significantly decreased expression in aging mice hearts (Fig. 7D and S6A-B) and *Hand1*, *Hand2* and *Nkx2*.5 significantly decreased in expression in aging non-human primate rhesus macaque hearts (Fig. 7E and S6C-D), when normalized to at least one of three different, stable housekeeping genes. These data suggest that the functional decline attributed to cardiomyocyte transcription factor loss in flies could be a conserved mechanism, caused in part by physical remodeling of the nucleus.

Discussion

The role nuclear remodeling has in heart function during natural aging has thus far been largely unexplored. Here, we demonstrate that CM nuclear remodeling, i.e., age-related loss of nuclear lamins, is intimately linked with tissue-level dysfunction. Genetically inducing nuclear remodeling leads to reduction in heart contractility, sarcomere disorganization and shortens lifespan by mimicking transcriptional changes that occur in natural aging. Our findings suggest that transcriptional misregulation downstream of nuclear remodeling may occur due to altered

chromatin accessibility and, strikingly, this represses CM fate transcription factors and sarcomeric structural components. Importantly, we show that preserving “youthful” nuclear properties, e.g., high Lamin expression and nuclear morphology, maintains CM transcription factor expression and heart function. These changes are conserved in both mice and non-human primates further demonstrating nuclear remodeling and myogenic transcriptional programs as potential therapeutic targets for preserving heart function during aging.

Our observations of age-associated nuclear remodeling in *Drosophila,* mice and non-human primates cardiomyocytes are in contrast to existing observations in *C. elegans* intestinal cells[35], *Drosophila* skeletal muscle[36], aged human fibroblasts[37] and what is currently understood for progeria-related laminopathies[19,23,33,37]. Rather than increasing in size and dysmorphia, we observe that aging CM nuclei atrophy and become rounder. We also, for the first time to our knowledge, demonstrate that CM nuclei stiffen upon aging *in situ*, an observation only seen previously in cell culture for progeria cells and only after multiple rounds of passaging[19]. Further supported by our assessment of non-cardiomyocyte ventral muscle nuclei that hypertrophy with age within the heart tube, our findings suggest that cardiomyocytes have specific mechanisms mediating nuclear remodeling.

In the context of *Drosophila* CMs, we sought to understand how nuclear remodeling occurred upon aging and identified that nuclear lamins, LamC and LamB, in addition to nesprin-related proteins Klar and Msp300, were downregulated upon aging. Consistent with our data, Lamin B has been previously reported to be downregulated with age[43,51,56] possibly due to its role in senesence[42], while a functional role for age-associated Lamin A/C reduction has not previously been explored. We found that genetically reducing LamC prematurely was sufficient to induce aging-like nuclear atrophy and increased circularity, but conversely, overexpression was required to change nuclear size in Xenopus and HeLa[25]. While A and B-type Lamins differentially contribute to nuclear mechanics[20], we observed that reduction of A-type LamC increased CM nuclear stiffness despite cultured cells’ nuclei soften with reduced Lamin A/C expression[20,26]. These differences could be accounted for by several hypotheses; First, *Drosophila* LamB and LamC could have differing functions compared to mammalian counterparts, although in other cell types, there is conservation between *Drosophila* and human Lamins[57]. Second, it is increasingly apparent that nuclei respond differently in 2D and 3D environments. In 2D cell culture, nuclear wrinkling indicates membrane laxity, whereas in 3D

environments[58,59], wrinkling is dependent on actin filaments intrusion into the perinuclear space and wrinkling infers high membrane tension[58]. Third, cell- or developmental-specific differences may result in alternative mechanics upon Lamin depletion. For example, Jevtic et al., show that in differentiated Xenopus cells, very high levels of Lamins can in fact decrease nuclear size[25]. Fourth, cell-specific LADs at the nuclear periphery show unique phenotypes upon Lamin A mutations in hiPSC-derived CMs versus adipocytes and hepatocytes[60]. Thus, differential Lamin-chromatin interactions could similarly contribute to altered mechanical regulation in aging cardiomyocytes verses other cell types.

Given the linkage of nuclear lamina to sarcomeres via the LINC complex and chromatin via LADs[61] as well as the functional deficits we uncovered, our data provide some of the first confirmation for a role for A-type Lamins in age-dependent regulation of heart function. Removal of Lamins disrupts chromatin attachment to the nuclear periphery, higher-order chromatin organization, and can influence gene expression[62–66]. These studies focus predominantly on stem cell fate and maturation, yet our data now suggests differences in postmitotic tissues. We identified that in both aging and LamC reduction, differentially accessible peaks were skewed towards decreased accessibility, despite evidence that heterochromatin is lost in Lamin A/C mutants and with aging[23,31]. Correspondingly, studies specifically disrupting LADs yield conflicting results depending on cell origin; Chang et al., reported chromatin decompaction and redistribution in breast cancer cells[66], while Ulianov et al., found that topological-associated domains decondensed but global chromatin density increased in embryonic-derived *Drosophila* S2 cells[64]. Similarly, maintaining lamina but disrupting chromatin attachment increased chromatin compaction in *C. elegans* embryos[65]. Disrupting LADs can also show localized alterations in accessibility, with recent work demonstrating Lamin B loss leads to repositioning of disease causing loci away from the nuclear periphery in post-mitotic neurones[67] and alter repressive H3K9me3 marks in *C. elegans*[68]. These conflicting instances, along with our data, suggest that accessibility both globally, and locally for specific loci, could be context specific, and thus our data suggests that in the context of aging, reduced accessibility could be coupled to dysfunction.

We show that ultimately, LamC-mediated nuclear remodeling appears to be a conserved process in vertebrates that reduces the expression of cardiomyocyte transcription factors, e.g., Hand/HAND1/2, Tin/NKX2-5 and H15/Tbx20. We observe that Hand specifically is less

accessible with aging and LamC reduction. In *Drosophila,* the highly conserved Tin is an early initiator of cardiogenesis and binds between Hand exons 3 and 4[69], an intron we observe to have reduced accessibility upon LamC reduction (Fig. 4F). Thus, reduced gene accessibility could further downregulate Hand and downstream myogenic transcription. We predict reduced chromatin accessibility might also account for the reduction of Tin/NKX2-5 and H15/Tbx20 with age across flies, mice, and monkeys. Our findings provide a new Lamin-mediated interpretation for previous observations of reduced NKX2-5 in aged, isolated mouse cardiomyocytes[70] and provides them with a role beyond development. We show in *Drosophila* that their adult-specific reduction gives rise to a marked reduction in heart function, supported by studies that find an adult-specific role for TBX20 when deleted in mice[71–73]. Consistent with these observations, CM transcription factors are misregulated in remodeling events leading to heart failure[74], e.g., HAND is downregulated in rodent hypertrophy[75] and in human cardiomyopathy[76]. Therefore, Lamin-mediated misregulation of myogenic transcriptional programs likely has a significant impact on mediating heart dysfunction during aging and may precede the development of heart failure. Since preserving LamC, and therefore nuclear morphology, maintained CM transcription factor expression and heart function despite aging in flies, our findings suggest nuclear lamina remodeling is a unique mechanism in age-related organ dysfunction. Furthermore, our work presents several avenues for investigating therapeutic interventions to increase health span into advanced age.

Methods

Drosophila melanogaster

Fly stocks were raised in non-crowded conditions on standard fly food medium consisting of yeast, cornstarch and molasses (10% yeast, 12% sugar and 1.5% agar). Flies were raised at 25°C except for the temperature sensitive fly crosses (HandGal4, TubGal80ts; TubGal80ts, Fig. 6) which were raised at 18°C until eclosure, then 50% of eclosed flies were aged at 29°C and 50% at 18°C. Freshly eclosed flies were collected and aged such that day of collection was day 1. Flies were transferred to fresh food every 2-3 days. Female flies were used for subsequent heart analysis to ensure consistent heart morphology. The following fly lines were used from the Bloomington stock center: *white-1118, w^{1118}*, *yellow-white yw, attp2; UAS-Luciferase* (#31603), *UAS-LamC RNAi* (#31621), *attp40* (#36304), *UAS-LamB RNAi* (#57501), *UAS-Stinger*-GFP

(#84277), *UAS-tinman RNAi* (#50663), *UAS-H15 RNAi* (#57415), *UAS-Hand RNAi* (#28977). *Hand$^{4.2}$Gal4* was acquired from Olsen Laboratory[69] and modified by the Bodmer lab to make *Hand$^{4.2}$Gal4, TubGal80^{ts}; TubGal80^{ts}*. *UAS-LamC* was gifted by the Walrath laboratory.

Mouse

All mouse experiments were performed in according to the guidelines established by the Institutional Animal Care and Use Committee at the University of California San Diego. Use of aged C57BL/6 mice was approved by the University of California San Diego Institutional Animal Care and Use Committee under study #S08172. All animals were provided with food and water *ad libitum* until the specific age time point at which point animals were euthanized by asphyxiation followed by cervical dislocation. The lower section of the left ventricle was removed from five young (5-month), three juvenile (9-month), four adult (14-month), and three aged (24-month) old mice and snap-frozen in liquid nitrogen immediately after resection and stored at -80^{o}C. The remainder of the heart was washed in PBS before embedding in OCT for cryosectioning. OCT boats containing hearts were frozen on dry ice with methyl butane before storage at -80^{o}C.

Rhesus Macaque

Ten adult male rhesus monkeys (ages: 8.87, 9.7, 10.66, 12.88, 14.12, 18.81, 19.59, 23.39, 24.73, and 25.48 years of age) were maintained at the NIA in accordance with NIH Institutional Animal Care and Use Committee protocol AG000238-07 (Effects of Aging on Experimental Atherosclerosis in Nonhuman Primates). Left ventricular samples from macaque where flash-frozen for qPCR analysis or formalin fixed, paraffin embedded and subsequently sectioned for immunofluorescence analysis.

Fly heart dissection

Flies were anaesthetized with FlyNap® (Carolina Biological Supply Co.) and dissected in artificial hemolymph that was oxygenated using aerators as previously described[52].

Immunofluorescence and imaging

Hearts dissected in oxygenated artificial hemolymph were relaxed using 10mM EGTA in oxygenated artificial hemolymph and immediately fixed with 4% formaldehyde in the same EGTA hemolymph solution for 20 minutes. The hearts were then rinsed 3 x with phosphate buffered saline (PBS) and washed 3 x 10 minutes with 0.5% Triton 100-X in PBS (PBST). The hearts were then blocked with 1% BSA in PBST (PBST-BSA) for 30 minutes. Primary antibodies were prepared as indicated below in PBST-BSA and incubated overnight at 4ºC. PBST and PBST-BSA washes were repeated and secondary antibody with DAPI and Phalloidin were prepared in PBST-BSA and incubated for 1.5-2 hours at room temperature. Following secondary incubation, the hearts were washed 3 x 20 minute with PBST and then rinsed 3 x with PBS to remove detergent. Antibodies and Dyes: Mouse anti-LamC (DSHB, LC28.26), 1:500. Mouse anti-LamB, 1:100 (DSHB, ADL195). Mouse anti-actinin (DSHB, 2G3-3D7) 1:100. DAPI (Sigma), 1:500. Rhodamine-Phalloidin (ThermoFisher, R415), 1:250. Donkey anti-mouse Alexa Fluor 488 (ThermoFisher, A21202), 1:500.

For imaging, the cuticle around the hearts was subsequently trimmed down to a small rectangle to prevent obstruction of the heart, then hearts were transferred to Fluormount® G slide mounting medium for antibody-based imaging or ProLong™ Glass Mountant (Invitrogen) for HCR imaging. The A2-A3 region of the heart was imaged on a Zeiss LSM780 inverted confocal microscope with a 40X objective, 1x Zoom, 0.44µm depth resolution for nuclear imaging or 0.88µm for actinin and HCR imaging, and at a resolution of 2148 x 1076 XY pixels.

Mouse heart sections embedded in OCT were cryosectioned and stored at -80ºC prior to fixation and staining. Slides were directly fixed with 4% PFA in PBS for 20 minutes at -20ºC with regular agitation to prevent freezing. Slides were subsequently washed 3 x 5 minutes with PBS and permeabilized for 1 hour with 1% PBS-Triton 100-X. Primary antibody was prepared in 10% Fetal Bovine Serum (FBS) with PBS (anti-Lamin A/C 1:250, Cell Signalling 4C11) and incubated overnight at 4ºC. Slides were subsequently washed 3 x 5 minutes with PBS before applying secondary antibody (Donkey anti-mouse Alexa Fluor 488, ThermoFisher, A21202, 1:500) and DAPI (Sigma). Slides were then washed 3 x 5 minutes with PBST and then PBS. Finally, samples were prepared for imaging using ProLong™ Glass Antifade Mountant (Invitrogen). Samples were

imaged on a Keyence All-in-One BZ-X Series Fluorescence Microscope, with a 60X objective, 1x Zoom, 1µm depth resolution and 1920 x 1440 XY pixel resolution.

Macaque heart sections were received from the NIA. For staining and imaging, slides were first rehydrated using the following steps: 2 x 10 minutes with Xylene, 100% ethanol, 95% ethanol (in DI water), 70% ethanol and 50% ethanol before rinsing with DI water. Slides were subsequently immersed in PBS with 0.5% Triton X-100 for 30 minutes and incubated with DAPI (Sigma) for 30 minutes, prior to 3 x 5 minute washes with PBST and 3 x 5 minutes with PBS. Slides were prepared using ProLong™ Glass Antifade Mountant (Invitrogen) and imaged as described for mouse heart sections.

Fly nuclear morphology and intensity analysis

For two-dimensional analysis of nuclear morphology, 3D stack images were acquired of the A2-A3 region of the heart as described above in the (Methods: Immunofluorescence and Imaging). The A2-A3 heart region possesses 3-4 cardiomyocyte pairs and therefore 6-8 total CM nuclei. Using ImageJ, the CM nuclei were cropped from the larger heart image, within a 22.17^2µm / 224^2pixel box with the minimal number of z slices to eliminate out-of-plane nuclei from the cuticle or ventral muscle overlaying the CM nucleus. The cropped nuclei were then segmented by the following function in a batch macro workflow:

```
//Setting the measurement parameters
run("Set Measurements...", "area perimeter fit display redirect=None decimal=3");

//Define directory
input = " ";
output = " ";

//For batch analysis
setBatchMode(true);
list = getFileList(input);
for (i = 0; i < list.length; i++)
```

```
        action(input, output, list[i]);
    setBatchMode(false);
    function action(input, output, filename) {

    //To open cropped nuclei stack
    open(input + filename);
        run("Z Project...", "projection=[Max Intensity]");

    //To save max projection image
        saveAs("Tiff", output+"Max_"+filename);

    //Set to the LamB or LamC channel
    Stack.setChannel(3);

    //To binarise image
    setAutoThreshold("IsoData dark");
    //setThreshold(68, 255);
        run("Convert to Mask", "method=IsoData background=Dark list");

    //For binary optimization
        run("Fill Holes", "slice");
        run("Open", "slice");
        run("Watershed", "slice");

    //To save max projection image
    saveAs("Tiff", output+"Binary_"+filename);
        run("Analyze Particles...", "size=20-Infinity display exclude add slice");
    }
```

The results were then saved and analyzed in excel. To calculate aspect ratio (AR) the minor axis was divided by the major axis and to calculate the circularity the excel function

"=(4*PI()*C2)/D2^2" was used. The data was presented, and the appropriate statistical tests performed in prism.

For three-dimensional analysis of nuclear morphology, the FIJI 3D Mesh plugin[80] was used on the LamC channel of the cropped nuclei stacks. The parameters for seeding and expanding the mesh were as follows: gamma, 200.0; pressure, 0.06; image weight, 0.05; beta 0.0; alpha, 1.0; steric neighbors, 0.0; divisions, 3.0. Volume and surface area from exported results were copied to prism for graphing and statistical testing.

The corrected total nuclear fluorescence (CTNF) was calculated using ImageJ. Cropped nuclear stacks, a binary image of the Lamin channel and max projection image were generated as described above in Nuclear Morphology Analysis. An ROI is generated from the binary and overlaid on the max projection image and area and integrated density are measured for the Lamin channel.

```
	//Setting the measurement parameters
	run("Set Measurements...", "area mean min integrated display redirect=None decimal=3");

	//Define directory
	PathMax = " ";
	PathBinary = " ";

	//Call lists
	listMax = getFileList(PathMax);
	listBinary = getFileList(PathBinary);

	for (i = 0; i < listBinary.length; i++){
		if(endsWith(listBinary[i], ".tif"))
		print(listBinary[i]);
```

```
        //Open binary image
        open(PathBinary+listBinary[i]);

        //Set to the Lamin Channel
        Stack.setChannel(3);

        //Generate ROI and close binary
        run("Analyze Particles...", "size=20.00-200.00 display add slice");
        close();

        //Open max projection image
        open(PathMax+listMax[i]);

        //Overlay ROI on max projection image
        roiManager("Select", 0);

        //Measure intensity of Lamin channel
        Stack.setChannel(3);
        run("Measure");

        //Reset for next image in list
        close();
        roiManager("Delete");
        }
```

Subsequently, to account for changes in nuclear size, the background is subtracted relative the area. A clear region outside of the nucleus is selected from the Lamin channel and the mean intensity measured. Then, the following equation is used to calculate the approximate protein amount: Corrected Total Nuclear Fluorescence = Integrated Density – (Mean Intensity x Nuclear Area).

Lamin localization

A custom python code[81] was modified to assess the intensity of Lamin at radially increasing distances from the center of the nucleus to the periphery for the max projected images also generated for nuclear morphology and intensity analysis (Figure S2F). The average mean intensity measurement at periphery was then divided by the average mean intensity the center to obtain the fold enrichment of Lamin at the periphery.

Sarcomere organization

Using ImageJ and confocal stack images of actinin stained hearts, the dorsal region of the A2-A3 region was projected to isolate a planar region of sarcomeres and eliminate actinin-stained sarcomeres from the ventral side of the CMs and ventral muscle. ROIs with a single layer of sarcomeres uninterrupted by non-CM cells were then cropped and saved. The isolated actinin regions from A2-A3 region were then batch processed using a published matlab code[53] which uses a scanning Fourier transform to calculate organizational index. The input parameters included a sarcomere length of 2.5-3.2μm, a sarcomere directionality of 90^{o}, a scanning resolution of 16 and at the appropriate pixel to μm ratio.

Lifespan assay

To determine lifespan, virgin females were collected and up to 30 flies separated into each vial. The flies were maintained at 25^{o}C and transferred to fresh food every 2-3 days, when dead flies were also counted.

Live heart imaging

Hearts were dissected as previously described[52] and heart function was assessed using high speed digital imaging (142fps, 9300 EM-CCD cameras, Hamamatsu), a 10X water-immersion lens and HCImageLive software (Hamamatsu). Using semi-automatic optical heart beat analysis software (SOHA)[82], fractional shortening was calculated from the end diastolic diameter (EDD) and end systolic diameters (ESD): (FS = EDD-ESD/EDD).

Nuclear extraction

30-60 dissected hearts were removed from their cuticle and transferred to 1ml of ice-cold Nuclei EZ lysis buffer (Sigma-Alrdich Nuclei EZ Prep isolation kit) in a 1ml glass douncer. 20 loose strokes followed by 10 minutes on ice and then 15 tight strokes aided dissociation of nuclei from the hearts. The solution was transferred to a low-bind Eppendorf and centrifuged at 500 x g for 5 minutes. The supernatant was removed, the nuclear pellet resuspended in fresh ice-cold Nuclei EZ lysis buffer and incubated on ice for 5 minutes. Spinning, removal of supernatant, resuspension and incubation on ice was repeated once more. The samples were then centrifuged once more at 500 x g before removing the supernatant and resuspending the pellet in PBS for nuclear AFM or Nuclei EZ storage buffer for ATAC Seq samples.

Atomic Force Microscopy

For atomic force microscopy, isolated nuclei in PBS were spun (500g, 3 minutes) on to 12mm coverslips coated with Poly-D-Lysine (1 µg/µl was used to coat coverslips for 5 minutes, then rinsed with purified water and left to dry overnight). Coverslips were transferred to a glass slide, secured with vacuum grease, and covered in a PBS droplet for AFM. Indentation experiments were performed on an MFP-3D Bio Atomic Force Microscope (Oxford Instruments) mounted in a Ti-U fluorescent inverted scope (Nikon Instruments, Melville, NY) and used Asylum Research 13, Igor Pro 6.34A software. Nanoworld PNP-TR tips were calibrated for their spring constant using the thermal noise method and used for probing isolated nuclei. A trigger force of 2nN, an approach Velocity constant of at 2 µm/s and a force distance of 6 µm were used to generate a force map with 12 points across 2µm^2. Hand4.2-Gal4 was used to drive expression of GFP, and thus only GFP-positive nuclei were selected for indentation. The software was used to calculate the Young's modulus using the Hertz equation[79]. Any poor fits to the indentation curve were excluded. Then, the average Young's modulus was calculated from the force map.

Bulk RNA sequencing

For gene expression analysis, corresponding adult flies were dissected as previously described[52] to expose the heart. Fat cells were carefully removed from either side of the length of the heart. A minimum of 15 hearts were then pulled from the cuticle using fine forceps and pooled together in Eppendorf tubes containing 300µl of Qiazol lysis reagent. Hearts were mechanically homogenized using a handheld tissue homogenizer and plastic pestles. Afterward,

a further 400µl of Qiazol lysis reagent was added and the tube flash frozen in liquid nitrogen. Samples were stored for up to 2 weeks at -80ºC until RNA extraction was performed. Total RNA was then extracted and purified using the Qiagen miRNeasy Mini kit (Cat. No. 217004) as per the protocol. The purified RNA was then processed by the Institute for Genomic Medicine at University California San Diego. RNA integrity was analyzed using an Agilent Tape station system and precise RNA concentration determined using a Qubit 2.0 Fluorometer. Libraries were built using the Illumina TruSeq Stranded RNA, High Throughput Library Prep Kit and sequenced on a NovaSeq 6000 for samples with RIN numbers at 9.0 and above.

RNA-Sequencing data was analyzed by ROSALIND® (https://rosalind.onramp.bio/), with a HyperScale architecture developed by ROSALIND, Inc. (San Diego, CA). Reads were trimmed using cutadapt[83]. Quality scores were assessed using FastQC[84]. Reads were aligned to the Drosophila melanogaster genome build dm6 using STAR[85]. Individual sample reads were quantified using HTseq[86] and normalized via Relative Log Expression (RLE) using DESeq2 R library[87]. Read Distribution percentages, violin plots, identity heatmaps, and sample MDS plots were generated as part of the QC step using RSeQC[88]. DEseq2 was also used to calculate fold changes and p-values and perform optional covariate correction. Clustering of genes for the final heatmap of differentially expressed genes was done using the PAM (Partitioning Around Medoids) method using the fpc R library[89]. Hypergeometric distribution was used to analyze the enrichment of pathways, gene ontology, domain structure, and other ontologies. The topGO R library[90,] was used to determine local similarities and dependencies between GO terms in order to perform Elim pruning correction. Several database sources were referenced for enrichment analysis, including Interpro[91], NCBI[92] MSigDB[93,94], REACTOME[95], WikiPathways[96]. Enrichment was calculated relative to a set of background genes relevant for the experiment. Panther was used to assess GO terms for gene lists generated in Rosalind.

Hybridization Chain Reaction (HCR)

Hearts were dissected as previously described[52] to expose the heart in a 2.5mm dish. The hearts were relaxed with 10mM EGTA in oxygenated hemolymph and fixed with 4% formaldehyde in 0.1% Tween 20, PBS for 20 minutes. Next, the hearts were washed 2 x 5 minutes with 0.1% Tween 20, PBS. Then on ice, hearts were incubated, each for 5 minutes, with 25%, 50%, 75%,

100%, 75%, 50% and finally 25% methanol in PBS. Hearts were then permeabilized for 2 hours at room temperature with 1% Triton 100-X in PBS. A second fixation was repeated at room temperature and samples were washed 2 x 5 minutes with 0.1% Tween, PBS on ice. Then, a 50% 0.1% Tween 20, PBS; 50% 5X SSCT (20XSSC, 10% Tween 20, Ultrapure water) solution was used to wash the samples for 5 minutes on ice and replaced by 5X SSCT for a further 5 minutes. The cuticle with the heart attached was then trimmed down to a small rectangle and carefully transferred to a 96 well plate well (each containing a maximum of 7 hearts). Within the well, the hearts were incubated with probe hybridization buffer (Molecular Instruments) on ice for 5 minutes, then the plate was transferred to 37^{o}C for 30 minutes. 2µl of each probe designed by Molecular Instruments was prepared in 200µl of probe hybridization buffer and incubated overnight with the hearts at 37^{o}C. The following day, the samples were washed 4 x 15 minutes with probe wash buffer (Molecular Instruments); 2 x 5X SSCT and 1 x 5 minutes with amplification buffer (Molecular Instruments). To prepare the hairpins for fluorescence amplification, 2µl of corresponding h1 and h2 were heated to 95^{o}C for 90 seconds and cooled in the dark for 30 minutes. The cooled hairpins were then added to 100µl of amplification buffer and incubated with the hearts overnight at room temperature in the dark. On the next day, while maintained in the dark, the samples were washed 2 x 5 minutes with 5X SSCT; 2 x 30 minutes with 5X SSCT; 1 x 5 minutes with 5X SSCT and finally rinsed 3 x with PBS. DAPI (1:250) was added with the first 5X SSCT 30-minute wash or stained subsequently for 15 minutes in PBST, followed by 3 x 10-minute PBST washes and 3 x PBS rinses. Samples were prepared and imaged as described above (Methods section: Immunofluorescence and Imaging).

To quantify RNA expression levels, the processed hearts were imaged as described in the Immunofluorescence and Imaging section and then imported into ImageJ. For Hand, Tinman and H15 quantification, the A2-A3 heart region confocal stack was converted to a max projection, duplicated and then binarized. Using the max projected image as a guide, the cytoplasmic pockets surrounding the CM nuclei were then then traced, the ROI copied to the binary imaged for particle analysis. As the segmentation was imperfect for transcripts very close together and to account for differences in pocket size, the % area covered by the transcripts was used to assess statistical significance in Prism (Graphpad).

As Lamin C and B are expressed in cells other than the CM nuclei, i.e., the ventral muscle nuclei and the cuticle, the narrowest stacks were taken around the nuclear-cytoplasmic pocket to eliminate interfering non-CM transcripts, and then the same analysis was conducted as for H15, Tinman and H15. The macro is as follows:

```
//Generate max projection image of the confocal stack image
run("Z Project...", "projection=[Max Intensity]");
Stack.setDisplayMode("composite");

//Maintains a copy of the max projection image
run("Duplicate...", "duplicate");

//Binarize the max projection image
run("Subtract Background...", "rolling=5 stack");
run("Gaussian Blur...", "sigma=1 stack");
setAutoThreshold("Triangle dark");
setOption("BlackBackground", true);
run("Convert to Mask", "method=Triangle background=Dark calculate black");
run("Watershed", "stack");
```

Bulk ATAC Sequencing

ATAC-seq was performed on 2,000-5,000 nuclei per sample. Samples were permeabilized in cold nuclear permeabilization buffer ((0.2% IGEPAL-CA630 (I8896, Sigma), 1 mM DTT (D9779, Sigma), Protease inhibitor (05056489001, Roche), and 5% BSA (A7906, Sigma) in PBS (10010-23, Thermo Fisher Scientific)) for 5 minutes on a rotator at 4°C followed by centrifugation for 5 min at 500g at 4°C. After decanting supernatant, the pellet was resuspended in cold tagmentation buffer ((33 mM Tris-acetate (pH = 7.8) (BP-152, Thermo Fisher Scientific), 66 mM K-acetate (P5708, Sigma), 11 mM Mg-acetate (M2545, Sigma), 16% DMF (DX1730, EMD Millipore) in molecular biology grade water (46000-CM, Corning)) followed by incubation with Tagmentation enzyme (FC-121-1030; Illumina) at 37°C with shaking at 500 rpm for 30 min. Tagmented DNA was purified using MinElute PCR purification kit (28004, QIAGEN). The

resulting libraries were amplified using NEBNext High-Fidelity 2X PCR Master Mix (M0541, NEB) with primer extension at 72°C for 5 minutes, denaturation at 98°C for 30 s, followed by 8 cycles of denaturation at 98°C for 10s, annealing at 63°C for 30s and extension at 72°C for 60s. After purification of amplified libraries using MinElute PCR purification kit (28004, QIAGEN), double sided size selection was performed using SPRIselect beads (B23317, Beckman Coulter) with 0.55X beads and 1.5X to sample volume.

Sample Processing from FASTQ - FASTQ files were submitted through the (redacted) Epigenetics ATAC-seq pipeline (https://github.com/(redacted)), based on the ENCODE pipeline. Briefly, reads were aligned using bowtie2, converted to uncompressed BAM files, sorted and index using: bowtie2-X2000 --mm --local -1 $fastq1 -2 $fastq2 | samtools view -Su /dev/stdin | samtools sort & index > xxx.PE2SE.bam &.bai 2> align.log. Poorly mapped, (<30 mapping score), duplicate, multimapped, and mitochondrial reads were removed using samtools and picard. Tn5 adapters were removed by truncating + end reads by 4 base pairs and – end reads by 5 base pairs, and then written to final output BAMs.

Computational Analysis - BAM files were downloaded from (redacted) Center for Epigenomics, sorted and indexed with samtools. Peakcalling was performed using MACS2 using the following commands: callpeak -f BAMPE -g dm - -q 0.01 --nomodel --shift -100 --extsize 200 --keep-dup all. MACS .xls output files and sorted BAMs were used to construct a Diffbind3.0.9 sample sheet for each comparison: 1- week vs 5-week w1118 samples, wildtype vs LamB iR attp40 samples, and wildtype vs LamC iR attp2 samples. Samples were read into R Studio using dba(), count densities per peak were calculated using dba.count(), filtering out peaks with <1 read per sample and a summit width of 100 (as recommended by the Diffbind3 vignette). Differential accessibility was calculated using the EdgeR wrapper of dba.analyze(). BED files were generated for each comparison using dba.report() and annotated using HOMER annotatePeaks.pl. Regions were filtered based on a log2 fold change of 0.32 and FDR of ≤ 0.1. Common features between comparisons were isolated using dplyr's inner_join function of the "Nearest.Refseq" column output of HOMER. Plots were generated using ggplot2 and ggrepel packages. Panther was used to assess GO terms for gene lists.

Quantitative PCR for Monkey and Mouse left ventricle

Total RNA was isolated from mouse and monkey frozen left ventricle sections by first, grinding frozen tissue in a pestle and mortar with liquid nitrogen to ensure samples did not degrade. Ground tissue was transferred to an Eppendorf and resuspended in 600ul of RLT lysis buffer from the RNeasy mini RNA extraction kit (Qiagen). The suspension was then transferred to a QIAshredder column and centrifuged at <10,000 rcf for 5 minutes for further homogenization. The supernatant was collected and total RNA was extracted using the RNAeasy mini RNA extraction kit (Qiagen) as per the protocol. RNA quality was assessed using an Agilent Tape station system. Poly(A)$^{+}$ RNA was reverse transcribed using oligo(dT) reagent of the SuperScript IV First-Strand Synthesis kit (Thermofisher) and cDNA library generated using manufacturers protocol with a final RNase step. RT-qPCR was then performed in triplicate for each sample using SYBR Green PCR Master mix (Thermofisher) and the CFX96 hardware (Biorad). Each gene of interest was normalized to three housekeeping genes[77,78] using the delta CT equation $2^{-(AvgCqGOI - AvgCqHK)}$. Primer sequences are shown in Table S10 and validated for specificity by melt temperature, and efficiency by DNA concentration titration are shown below.

Statistical analysis

Microsoft Excel 2011, Matlab 2020a, Python and Prism 9 Software were used to present data and conduct statistical analysis. The respective statistical tests and n numbers are described in the figure legends. For nuclear morphology and intensity analysis and HCR, 6-8 nuclei were cropped from the A2-A3 heart section and a minimum of 7 hearts were assessed. For RNA extraction, 15 hearts were collected per condition, and at least three biological replicated were acquired. For nuclear extraction 30-50 hearts were extracted per condition and 3-5 replicates were obtained. For SOHA live heart imaging, >13 hearts were imaged and analyzed. For actinin organization, >14 hearts were analyzed. For lifespan assays, more than 100 flies were recorded. The following statistical significance cut off was applied: n.s. $p>0.05$, * $p<0.05$, **$p<0.01$, ***$p<0.01$, ****$p<0.0001$. No tests were conducted to measure statistical power or normality of distributions.

Data and code availability

Software to image fly hearts, analyze their contraction, and create kymographs, i.e., Semi-automatic Optical Heartbeat Analysis, SOHA, is available at http://sohasoftware.com/index.html. Python code to assess Lamin distribution is available at (redacted). Any ImageJ macros have been included in Quantification and Statistical Analysis Section in Materials and Methods. RNA-Seq and ATAC-Seq data is deposited at Gene Omnibus Express (GEO) Accession GSE (redacted) and GSE (redacted), respectively.

Acknowledgements

Redacted.

Author Contributions

Redacted.

Competing Interests

The authors declare no competing interests.

References

1. Phillip, J. M., Aifuwa, I., Walston, J. & Wirtz, D. The Mechanobiology of Aging. *Annu Rev Biomed Eng* **17**, 113–141 (2015).
2. Gilbert, H. T. J. & Swift, J. The consequences of ageing, progeroid syndromes and cellular senescence on mechanotransduction and the nucleus. *Exp Cell Res* **378**, 98–103 (2019).
3. CDC, N. Underlying Cause of Death 1999-2013 on CDC WONDER Online Database, released 2015. Data are from the Multiple Cause of Death Files, 1999-2013, as compiled from data provided by the 57 vital statistics jurisdictions through the Vital Statistics Cooperative . (2015).
4. Sessions, A. O. *et al.* Extracellular matrix downregulation in the Drosophila heart preserves contractile function and improves lifespan. *Matrix Biol* **62**, 15–27 (2017).
5. Kaushik, G. *et al.* Vinculin network-mediated cytoskeletal remodeling regulates contractile function in the aging heart. *Sci Transl Med* **7**, 292ra99 (2015).
6. Sessions, A. O. & Engler, A. J. Mechanical Regulation of Cardiac Aging in Model Systems. *Circ Res* **118**, 1553–1562 (2016).

7. Birks, E. J. Molecular changes after left ventricular assist device support for heart failure. *Circ. Res.* **113**, 777–791 (2013).
8. Van Berlo, J. H. *et al.* C-kit+ cells minimally contribute cardiomyocytes to the heart. *Nature* **509**, 337–341 (2014).
9. Cho, S., Irianto, J. & Discher, D. E. Mechanosensing by the nucleus: From pathways to scaling relationships. *J Cell Biol* **216**, 305–315 (2017).
10. Janota, C. S., Calero-Cuenca, F. J. & Gomes, E. R. The role of the cell nucleus in mechanotransduction. *Current Opinion in Cell Biology* vol. 63 204–211 (2020).
11. Saucerman, J. J., Tan, P. M., Buchholz, K. S., McCulloch, A. D. & Omens, J. H. Mechanical regulation of gene expression in cardiac myocytes and fibroblasts. *Nature Reviews Cardiology* vol. 16 361–378 (2019).
12. Khatau, S. B. *et al.* A perinuclear actin cap regulates nuclear shape. *Proc. Natl. Acad. Sci. U. S. A.* **106**, 19017–19022 (2009).
13. Ramdas, N. M. & Shivashankar, G. V. Cytoskeletal Control of Nuclear Morphology and Chromatin Organization. *J. Mol. Biol.* **427**, 695–706 (2015).
14. Stephens, A. D., Banigan, E. J., Adam, S. A., Goldman, R. D. & Marko, J. F. Chromatin and lamin A determine two different mechanical response regimes of the cell nucleus. *Mol Biol Cell* **28**, 1984–1996 (2017).
15. Stephens, A. D. *et al.* Chromatin histone modifications and rigidity affect nuclear morphology independent of lamins. *Mol Biol Cell* **29**, 220–233 (2018).
16. van Steensel, B. & Belmont, A. S. Lamina-Associated Domains: Links with Chromosome Architecture, Heterochromatin, and Gene Repression. *Cell* **169**, 780–791 (2017).
17. Dahl, K. N., Ribeiro, A. J. & Lammerding, J. Nuclear shape, mechanics, and mechanotransduction. *Circ Res* **102**, 1307–1318 (2008).
18. Chatzifrangkeskou, M., Kah, D., Lange, J. R., Goldmann, W. H. & Muchir, A. Mutated lamin A modulates stiffness in muscle cells. *Biochem. Biophys. Res. Commun.* (2020) doi:10.1016/j.bbrc.2020.05.102.
19. Verstraeten, V. L. R. M., Ji, J. Y., Cummings, K. S., Lee, R. T. & Lammerding, J. Increased mechanosensitivity and nuclear stiffness in Hutchinson–Gilford progeria cells: effects of farnesyltransferase inhibitors. *Aging Cell* **7**, 383–393 (2008).
20. Lammerding, J. *et al.* Lamins a and C but not lamin B1 regulate nuclear mechanics. *J. Biol. Chem.* **281**, 25768–25780 (2006).
21. Srivastava, L. K., Ju, Z., Ghagre, A. & Ehrlicher, A. J. Spatial distribution of lamin A determines nuclear stiffness and stress-mediated deformation. *bioRxiv* 1–15 (2019) doi:10.1101/765263.

22. Buxboim, A. *et al.* Matrix elasticity regulates lamin-A,C phosphorylation and turnover with feedback to actomyosin. *Curr. Biol.* **24**, 1909–1917 (2014).
23. Dahl, K. N. *et al.* Distinct structural and mechanical properties of the nuclear lamina in Hutchinson-Gilford progeria syndrome. *Proc. Natl. Acad. Sci. U. S. A.* **103**, 10271–10276 (2006).
24. Brandt, A. *et al.* Developmental control of nuclear size and shape by kugelkern and kurzkern. *Curr. Biol.* **16**, 543–552 (2006).
25. Jevtić, P. *et al.* Concentration-dependent effects of nuclear lamins on nuclear size in xenopus and mammalian cells. *J. Biol. Chem.* **290**, 27557–27571 (2015).
26. Pajerowski, J. D., Dahl, K. N., Zhong, F. L., Sammak, P. J. & Discher, D. E. Physical plasticity of the nucleus in stem cell differentiation. *Proc. Natl. Acad. Sci. U. S. A.* **104**, 15619–15624 (2007).
27. Bonne, G. *et al.* Mutations in the gene encoding lamin A/C cause autosomal dominant Emery-Dreifuss muscular dystrophy. *Nat. Genet.* **21**, 285–288 (1999).
28. Di Barletta, M. R. *et al.* Different mutations in the LMNA gene cause autosomal dominant autosomal recessive Emery-Dreifuss muscular dystrophy. *Am. J. Hum. Genet.* **66**, 1407–1412 (2000).
29. R.G, T. M. *et al.* Natural history of dilated cardiomyopathy due to lamin A/C gene mutations. *J. Am. Coll. Cardiol.* **41**, 771–780 (2003).
30. Capell, B. C., Collins, F. S. & Nabel, E. G. Mechanisms of cardiovascular disease in accelerated aging syndromes. *Circ Res* **101**, 13–26 (2007).
31. Scaffidi, P. & Misteli, T. Reversal of the cellular phenotype in the premature aging disease Hutchinson-Gilford progeria syndrome. *Nat. Med.* **11**, 440–445 (2005).
32. Liu, B. *et al.* Genomic instability in laminopathy-based premature aging. *Nat. Med.* **11**, 780–785 (2005).
33. Goldman, R. D. *et al.* Accumulation of mutant lamin A progressive changes in nuclear architecture in Hutchinson-Gilford progeria syndrome. *Proc. Natl. Acad. Sci. U. S. A.* **101**, 8963–8968 (2004).
34. Shumaker, D. K. *et al.* Mutant nuclear lamin A leads to progressive alterations of epigenetic control in premature aging. *Proc. Natl. Acad. Sci.* **103**, 8703 (2006).
35. Haithcock, E. *et al.* Age-related changes of nuclear architecture in Caenorhabditis elegans. *Proc Natl Acad Sci U S A* **102**, 16690–16695 (2005).
36. Brandt, A., Krohne, G. & Großhans, J. The farnesylated nuclear proteins KUGELKERN and LAMIN B promote aging-like phenotypes in Drosophila flies. *Aging Cell* **7**, 541–551 (2008).
37. Scaffidi, P. & Misteli, T. Lamin A-dependent nuclear defects in human aging. *Science (80-.).* **312**, 1059–1063 (2006).

38. Larson, K. *et al.* Heterochromatin formation promotes longevity and represses ribosomal RNA synthesis. *PLoS Genet.* **8**, (2012).
39. McClintock, D. *et al.* The Mutant Form of Lamin A that Causes Hutchinson-Gilford Progeria Is a Biomarker of Cellular Aging in Human Skin. *PLoS One* **2**, e1269 (2007).
40. Messner, M. *et al.* Upregulation of the aging related LMNA splice variant progerin in dilated cardiomyopathy. *PLoS One* **13**, e0196739 (2018).
41. Afilalo, J. *et al.* Age-related changes in lamin A/C expression in cardiomyocytes. *Am. J. Physiol. Circ. Physiol.* **293**, H1451–H1456 (2007).
42. Freund, A., Laberge, R. M., Demaria, M. & Campisi, J. Lamin B1 loss is a senescence-associated biomarker. *Mol. Biol. Cell* **23**, 2066–2075 (2012).
43. Chen, H., Zheng, X. & Zheng, Y. Age-associated loss of lamin-b leads to systemic inflammation and gut hyperplasia. *Cell* **159**, 829–843 (2014).
44. Han, L. *et al.* Lamin B2 Levels Regulate Polyploidization of Cardiomyocyte Nuclei and Myocardial Regeneration. *Dev Cell* (2020) doi:10.1016/j.devcel.2020.01.030.
45. Nikolova, V. *et al.* Defects in nuclear structure and function promote dilated cardiomyopathy in lamin A/C–deficient mice. *J. Clin. Invest.* **113**, 357–369 (2004).
46. Cammarato, A. *et al.* A mighty small heart: the cardiac proteome of adult Drosophila melanogaster. *PLoS One* **6**, e18497 (2011).
47. Nishimura, M. *et al.* A dual role for integrin-linked kinase and β1-integrin in modulating cardiac aging. *Aging Cell* **13**, 431–440 (2014).
48. Nava, M. M. *et al.* Heterochromatin-Driven Nuclear Softening Protects the Genome against Mechanical Stress-Induced Damage. *Cell* (2020) doi:10.1016/j.cell.2020.03.052.
49. Prakash, A. *et al.* Cardiac abnormalities in patients with hutchinson-gilford progeria syndrome. *JAMA Cardiol.* **3**, 326–334 (2018).
50. Choi, H. M. T. *et al.* Third-generation in situ hybridization chain reaction: Multiplexed, quantitative, sensitive, versatile, robust. *Dev.* **145**, 1–10 (2018).
51. bin Imtiaz, M. K. *et al.* Declining lamin B1 expression mediates age-dependent decreases of hippocampal stem cell activity. *Cell Stem Cell* **28**, 967-977.e8 (2021).
52. Vogler, G. & Ocorr, K. Visualizing the beating heart in Drosophila. *J. Vis. Exp.* 1425 (2009) doi:10.3791/1425.
53. Salick, M. R. *et al.* The scanning gradient Fourier transform (SGFT) method for assessing sarcomere organization and alignment. *J. Appl. Phys.* **127**, 194701 (2020).
54. Cheedipudi Sirisha, M. *et al.* Genomic Reorganization of Lamin-Associated Domains in Cardiac Myocytes Is Associated With Differential Gene Expression and DNA Methylation in Human

Dilated Cardiomyopathy. *Circ Res* **124**, 1198–1213 (2019).
55. Davidson, E. H. & Erwin, D. H. Gene Regulatory Networks and the Evolution of Animal Body Plans. *Science (80-.).* **311**, 796 LP – 800 (2006).
56. Dreesen, O. *et al.* Lamin B1 fluctuations have differential effects on cellular proliferation and senescence. *J. Cell Biol.* **200**, 605–617 (2013).
57. Schulze, S. R. *et al.* A comparative study of Drosophila and human A-type lamins. *PLoS One* **4**, (2009).
58. Cosgrove, B. D. *et al.* Nuclear envelope wrinkling predicts mesenchymal progenitor cell mechano-response in 2D and 3D microenvironments. *Biomaterials* **270**, 120662 (2021).
59. Nava, M. M. *et al.* Heterochromatin-Driven Nuclear Softening Protects the Genome against Mechanical Stress-Induced Damage. *Cell* **181**, 800-817.e22 (2020).
60. Rhoades, J. H., Prosser, B. L. & Musunuru, K. Pathogenic LMNA variants disrupt cardiac lamina-chromatin interactions and de-repress alternative fate genes Article Pathogenic LMNA variants disrupt cardiac lamina-chromatin interactions and de-repress alternative fate genes. *Stem Cell* 1–17 (2021) doi:10.1016/j.stem.2020.12.016.
61. van Steensel, B. & Belmont, A. S. Lamina-Associated Domains: Links with Chromosome Architecture, Heterochromatin, and Gene Repression. *Cell* **169**, 780–791 (2017).
62. Zheng, X. *et al.* Lamins Organize the Global Three-Dimensional Genome from the Nuclear Periphery. *Mol. Cell* **71**, 802-815.e7 (2018).
63. Hu, B. *et al.* Plant lamin-like proteins mediate chromatin tethering at the nuclear periphery. *Genome Biol.* **20**, 1–18 (2019).
64. Ulianov, S. V *et al.* Nuclear lamina integrity is required for proper spatial organization of chromatin in Drosophila. *Nat Commun* **10**, 1176 (2019).
65. Sawh, A. N. *et al.* Lamina-Dependent Stretching and Unconventional Chromosome Compartments in Early C. elegans Embryos. *Mol. Cell* **78**, 96-111.e6 (2020).
66. Chang, L. *et al.* Nuclear peripheral chromatin-lamin B1 interaction is required for global integrity of chromatin architecture and dynamics in human cells. *Protein Cell* (2020) doi:10.1007/s13238-020-00794-8.
67. Noguchi, A. *et al.* Decreased Lamin B1 Levels Affect Gene Positioning and Expression in Postmitotic Neurons. *Neurosci. Res.* (2021) doi:https://doi.org/10.1016/j.neures.2021.05.011.
68. Li, C.-L. *et al.* Region-specific H3K9me3 gain in aged somatic tissues in Caenorhabditis elegans. *PLOS Genet.* **17**, e1009432 (2021).
69. Han, Z. & Olson, E. N. Hand is a direct target of Tinman and GATA factors during Drosophila cardiogenesis and hematopoiesis. *Development* **132**, 3525–3536 (2005).

70. Bodyak, N. Gene expression profiling of the aging mouse cardiac myocytes. *Nucleic Acids Res.* **30**, 3788–3794 (2002).
71. Shen, T. *et al.* Tbx20 regulates a genetic program essential to adult mouse cardiomyocyte function. *J. Clin. Invest.* **121**, 4640–4654 (2011).
72. Sakabe, N. J. *et al.* Dual transcriptional activator and repressor roles of TBX20 regulate adult cardiac structure and function. *Hum. Mol. Genet.* **21**, 2194–2204 (2012).
73. Stennard, F. A. *et al.* Murine T-box transcription factor Tbx20 acts as a repressor during heart development, and is essential for adult heart integrity, function and adaptation. *Development* **132**, 2451–2462 (2005).
74. Akazawa, H. & Komuro, I. Roles of cardiac transcription factors in cardiac hypertrophy. *Circ. Res.* **92**, 1079–1088 (2003).
75. Thattaliyath, B. D., Livi, C. B., Steinhelper, M. E., Toney, G. M. & Firulli, A. B. HAND1 and HAND2 are expressed in the adult-rodent heart and are modulated during cardiac hypertrophy. *Biochem. Biophys. Res. Commun.* **297**, 870–875 (2002).
76. Natarajan, A. *et al.* Human eHAND, but not dHAND, is down-regulated in cardiomyopathies. *J. Mol. Cell. Cardiol.* **33**, 1607–1614 (2001).
77. Ahn, K. *et al.* Selection of internal reference genes for SYBR green qRT-PCR studies of rhesus monkey (Macaca mulatta) tissues. *BMC Mol. Biol.* **9**, 1–8 (2008).
78. Ruiz-Villalba, A. *et al.* Reference genes for gene expression studies in the mouse heart. *Sci. Rep.* **7**, 1–9 (2017).
79. Hertz, H. Ueber den kontakt elastischer koerper. *J. fuer die Reine Angew. Math.* **92**, 156 (1881).
80. Smith, M. B., Chaigne, A. & Paluch, E. K. An active contour ImageJ plugin to monitor daughter cell size in 3D during cytokinesis. *Methods Cell Biol* **137**, 323–340 (2017).
81. Beri, P. *et al.* Cell adhesiveness serves as a biophysical marker for metastatic potential. *Cancer Res.* canres.1794.2019 (2019) doi:10.1158/0008-5472.CAN-19-1794.
82. Ocorr, K., Fink, M., Cammarato, A., Bernstein, S. & Bodmer, R. Semi-automated Optical Heartbeat Analysis of small hearts. *J. Vis. Exp.* 1435 (2009) doi:10.3791/1435.
83. Martin, M. Cutadapt removes adapter sequences from high-throughput sequencing reads. *EMBnet.journal* **17**, 10–12 (2011).
84. Babraham Bioinformatics - FastQC A Quality Control tool for High Throughput Sequence Data. https://www.bioinformatics.babraham.ac.uk/projects/fastqc/.
85. Dobin, A. *et al.* STAR: ultrafast universal RNA-seq aligner. *Bioinformatics* **29**, 15–21 (2013).
86. S, A., PT, P. & W, H. HTSeq--a Python framework to work with high-throughput sequencing data. *Bioinformatics* **31**, 166–169 (2015).

87. Love, M. I., Huber, W. & Anders, S. Moderated estimation of fold change and dispersion for RNA-seq data with DESeq2. *Genome Biol. 2014 1512* **15**, 1–21 (2014).
88. L, W., S, W. & W, L. RSeQC: quality control of RNA-seq experiments. *Bioinformatics* **28**, 2184–2185 (2012).
89. CRAN - Package fpc. https://cran.r-project.org/web/packages/fpc/index.html.
90. Bioconductor - topGO. https://bioconductor.org/packages/release/bioc/html/topGO.html.
91. Mitchell, A. L. *et al.* InterPro in 2019: improving coverage, classification and access to protein sequence annotations. *Nucleic Acids Res.* **47**, D351–D360 (2019).
92. LY, G. *et al.* The NCBI BioSystems database. *Nucleic Acids Res.* **38**, (2010).
93. Subramanian, A. *et al.* Gene set enrichment analysis: A knowledge-based approach for interpreting genome-wide expression profiles. *Proc. Natl. Acad. Sci.* **102**, 15545–15550 (2005).
94. Liberzon, A. *et al.* Molecular signatures database (MSigDB) 3.0. *Bioinformatics* **27**, 1739 (2011).
95. A, F. *et al.* The Reactome Pathway Knowledgebase. *Nucleic Acids Res.* **46**, D649–D655 (2018).
96. DN, S. *et al.* WikiPathways: a multifaceted pathway database bridging metabolomics to other omics research. *Nucleic Acids Res.* **46**, D661–D667 (2018).

Figure Legends

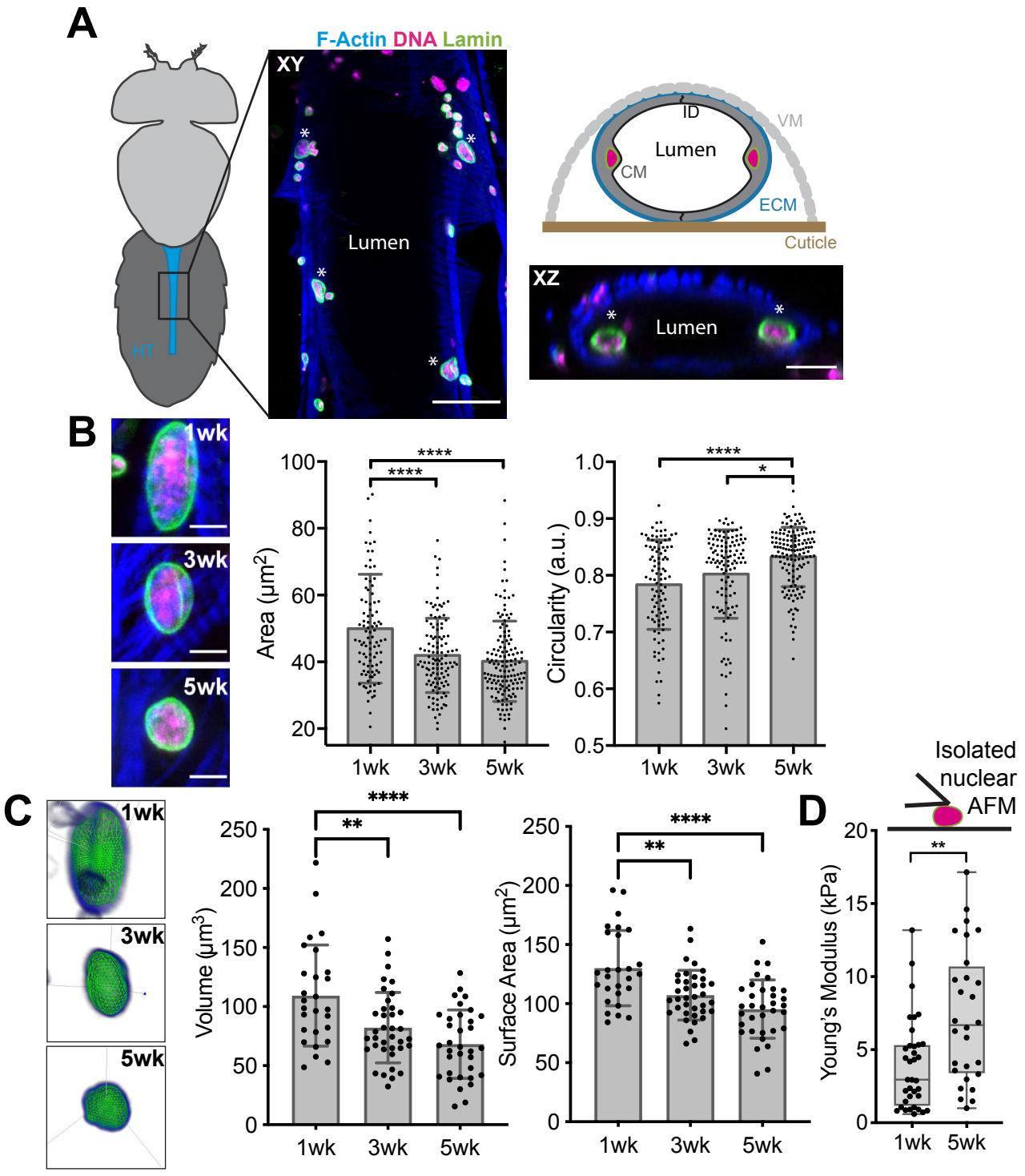

Figure 1: Age-Associated Changes in Cardiac Nuclear Morphology and Mechanics. (A) Schematic of ventral *Drosophila* body plan with the heart tube in the abdomen highlighted in blue. Expanded view of the heart tube shows a coronal (XY) confocal section through the heart

tube (center) as well as a transverse (XZ) confocal section and schematic to highlight nuclear position in the luminal space (right). Asterisks indicate cardiomyocyte nuclei. Scale bar is 20 μm. **(B)** Images of w^{1118} fly nuclei (left) and plot of their corresponding 2D projection data (right). Scale bar is 5 μm. n = 96, 116, and 141 nuclei for 1- , 3-, and 5-week adults, respectively. **(C)** 3D renderings of cardiac nuclei (left) and their corresponding for volume and surface area. n = 27, 37, and 34 nuclei for 1- , 3-, and 5-week adult w^{1118} flies respectively. **(D)** Atomic force microscopy (AFM) nuclear indentation schematic (top) and plot of stiffness values, i.e., Young's modulus, for nuclei of w^{1118} flies (bottom). n = 35 and 28 nuclei for 1- and 5-week adults, respectively. **$p<10^{-2}$ and ****$p<10^{-4}$ by one-way ANOVA with Tukey multiple comparisons test in (B-C) and unpaired t-test with Welch's correction in (D).

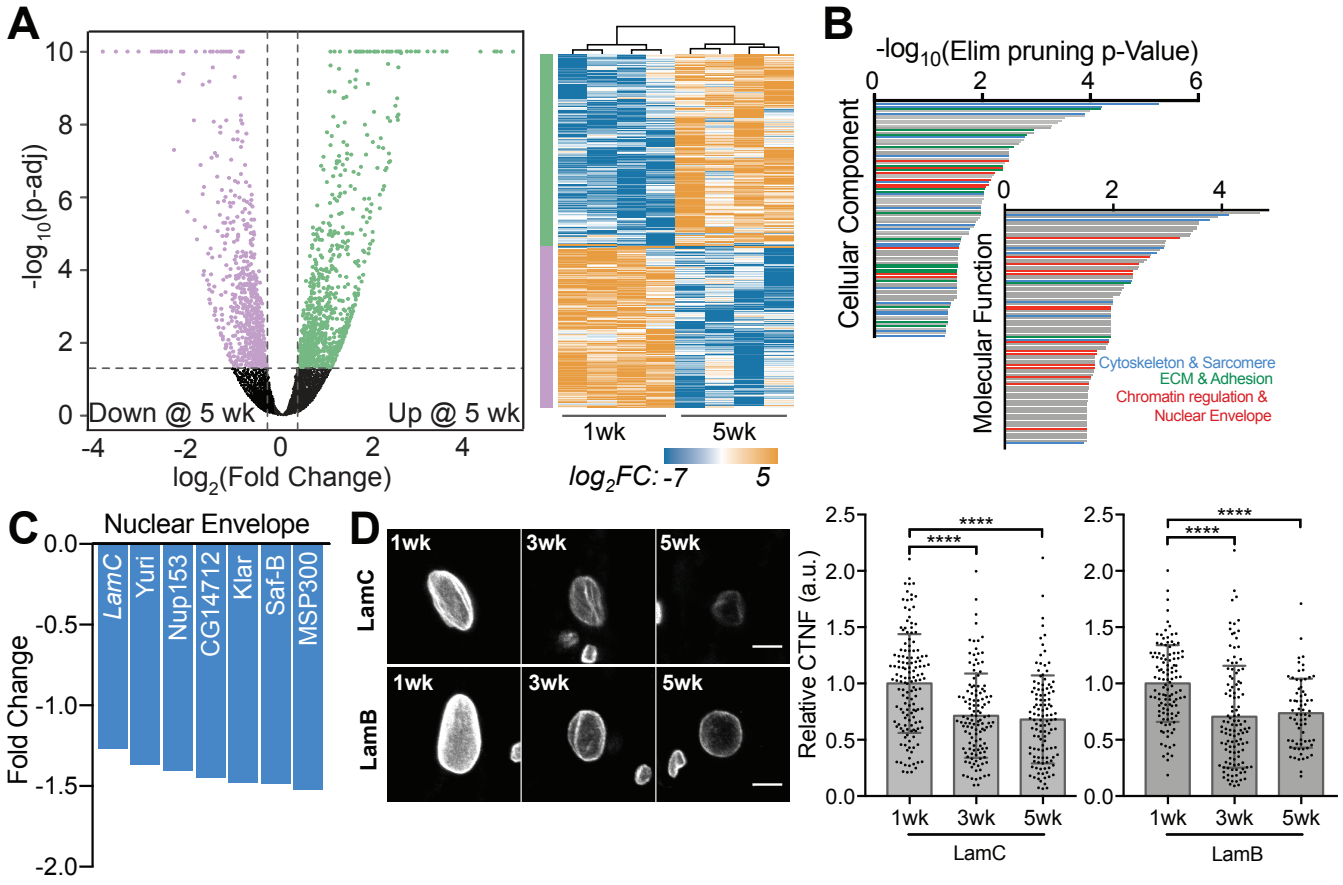

Figure 2: Natural Aging Downregulates Nuclear Envelope Proteins. (A) Volcano plot and heat map of bulk RNA-seq from surgically dissected heart tubes. Fold change (FC) represents 5-week w^{1118} fly hearts normalized to 1-week old hearts and p-adjusted was computed from quadruplicate repeats. 1,268 differentially expressed genes (DEGs) were assessed from cutoffs of -1.25 > FC > 1.25 and p-adj < 0.05 (dashed lines) from comparisons of 15 fly hearts in quadruplicate biological replicates; DEGs increasing and decreasing with age are shown in green and purple, respectively. **(B)** The top 100 molecular function and cellular component gene ontological terms are plotted based on elimination pruning p-value. Terms related to cytoskeleton & sarcomere, ECM & adhesion, and chromatin remodeling & nuclear envelope are annotated by color. **(C)** Expression of selected genes associated with nuclear envelope terms are plotted, with Lamin C (*LamC*) expression noted with italics. **(D)** Confocal projection images of cardiomyocyte nuclei showing Lamin B (*LamB*) and C expression with age (left). Scale bar is 5 μm. (right) Corrected total nuclear fluorescence (CTNF), which adjusts for nucleus size, is plotted for *LamB* and *LamC* as a function of adult fly age. n = 141, 124, 116, 114, 107, and 69 nuclei/condition

from left to right for LamC and LamB aged 1-, 3-, or 5-weeks of adulthood, respectively. ****$p<10^{-4}$ by one-way ANOVA with Tukey multiple comparisons test.

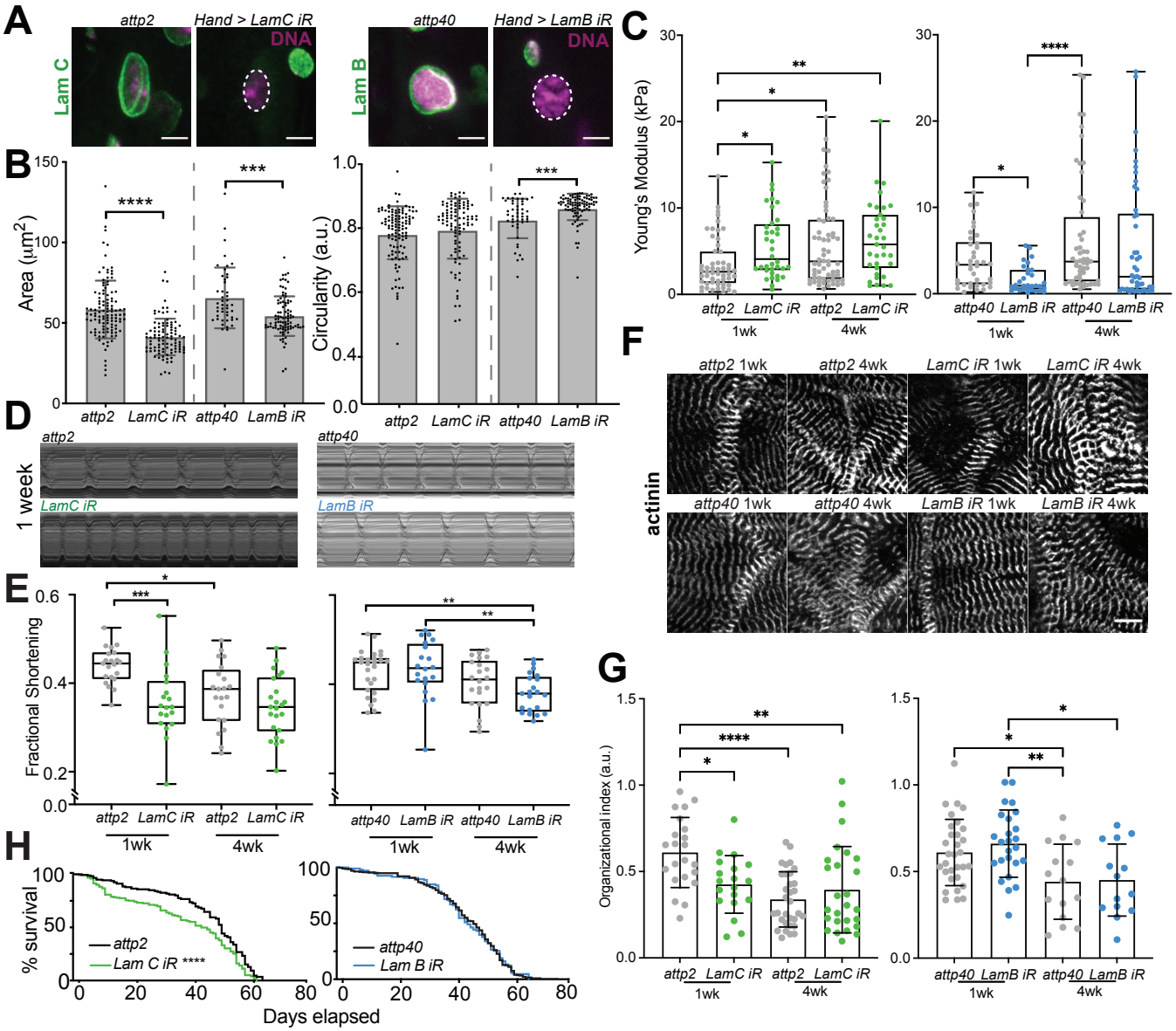

Figure 3: LamC, but not LamB, impacts Cardiomyocyte Aging, Heart Function, and Lifespan. (A) Confocal cross-section images are shown for transgenic flies knocking down *LamB* and *LamC* by RNAi (right) and their background fly line (left). Dashed lines indicate nuclear position based on DNA. Scale bar is 5 μm. **(B)** Plots quantifying nuclear area (left) and circularity (right) based on confocal images of *LamB* and *LamC* RNAi lines and their genetic control background at 1-week of adulthood. n = 111, 95, 46, and 90 (hearts/condition; left to right). **(C)** Plot of Young's modulus values is shown for nuclei of the indicated adult ages for *LamC* (green), *LamB* (blue) *RNAi*, and their control strains (grey). n = 53, 36, 63, 35, 38, 31, 52, and 46 (hearts/condition; left to right). **(D)** Representative kymographs of surgically exposed heart tubes

for *LamC* (green), *LamB* (blue) *RNAi*, and their control strains. **(E)** Fractional shortening at 1- and 4-weeks of adulthood is plotted for *LamC* (green) and *LamB* (blue) *RNAi*, and their control strains. n = 21,18, 21, 23, 27, 20, 22, and 20 (hearts/condition; left to right). **(F)** Representative images of α-actinin staining for the indicated transgenic flies and their control backgrounds (paired by row). Scale bar is 10 μm. **(G)** Organizational index is plotted for each heart tube. n = 22,19, 32, 26, 31, 25, 15, and 14 (hearts/condition; left to right). **(H)** Kaplan-Meier survival curve for *LamC* (green) and *LamB* (blue) *RNAi*, and their control strains. 102, 148, 95, and 200 flies for attp2, LamC RNAi, attp40, and LamB RNAi, respectively, were used in the plot. *$p<0.05$, **$p<10^{-2}$, ***$p<10^{-3}$, and ****$p<10^{-4}$ by one-way ANOVA with Tukey multiple comparisons test for (B-G). ****$p<10^{-4}$ based on Log-Rank (Mantel-Cox) test in (H).

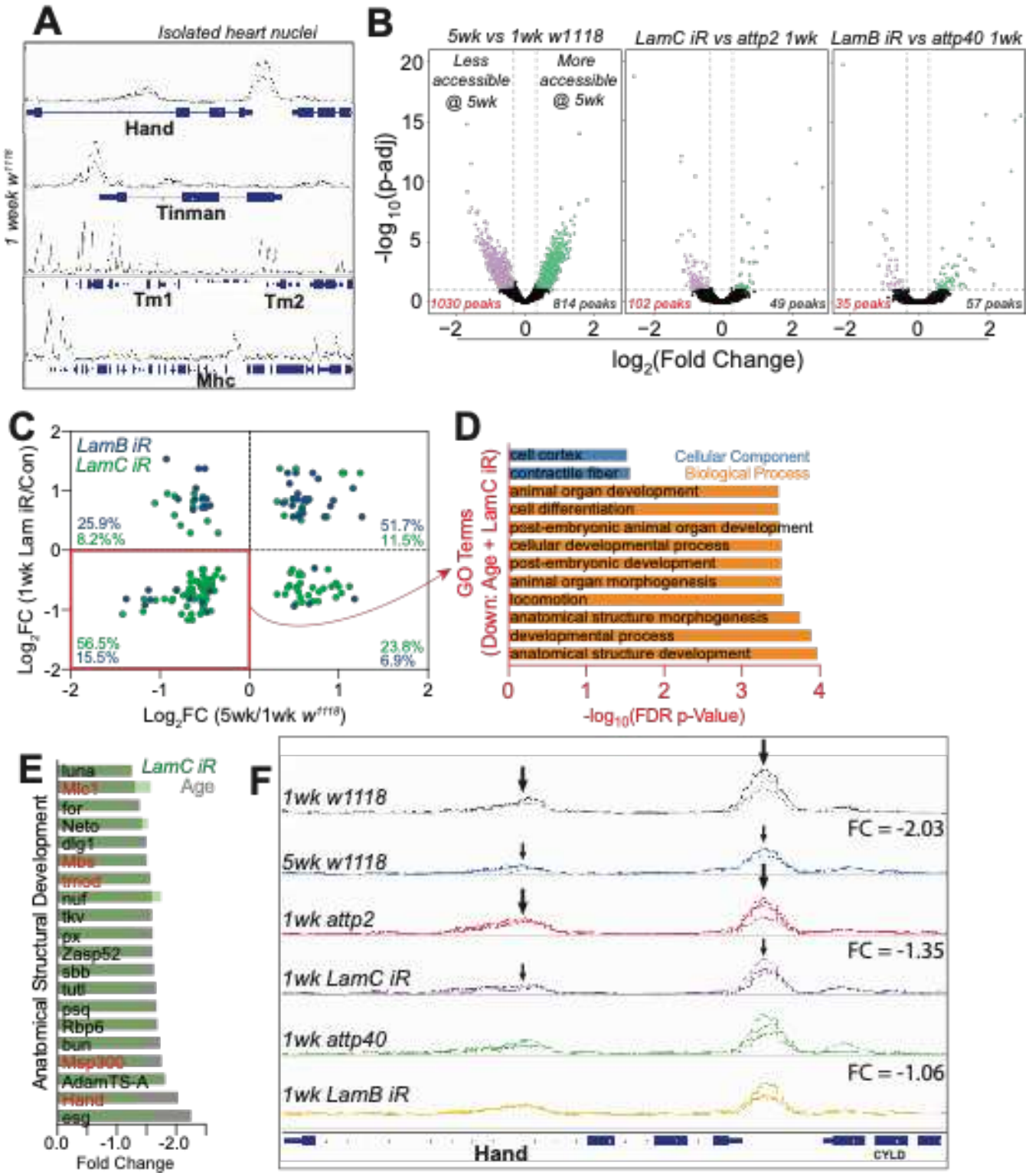

Figure 4: Chromatin Accessibility Decreases with Age and *LamC RNAi* at Sites of Myogenic Control. (A) Map of accessibility peaks for *Drosophila* cardiac transcription factor genes *Hand* (top) and *tinman (tin;* upper middle*)* and sarcomere genes *Tropomyosin* (*Tm1* and

Tm2; lower middle) and *Mhc* (bottom). Data is shown in triplicate sequencing runs using 1-week adult w^{1118} flies, i.e., 3 lines plotted in the panel. **(B)** Volcano plots of the indicated aging or transgenic comparisons of differentially accessible regions (DARs) from ATAC-seq. The number of peaks is annotated at the bottom for each comparison indicating if the region is more (black) or less (red) accessible relative to the comparator line. **(C)** Scatter plot is shown for ATAC-seq data comparing the fold change in accessibility for genes based on effects from aging and *LamC* (green) or *LamB* (blue) *RNAi*. Percentage of data in each quadrant are shown. **(D)** Top gene ontological terms are plotted for co-downregulated peaks (closest associated gene) in aged and *LamC RNAi* fly comparisons and ordered based on the false discovery rate p-value. **(E)** Genes within the anatomical structure term were plotted for their fold change for aging (gray) and *LamC RNAi* (green). Genes names in red represent myogenic transcription factors or muscle-specific structure proteins. **(F)** Map of accessibility peaks for the myogenic transcription factor *Hand*. Arrows indicate the location of a common DAR in *Hand* that is present and reduces in aged and *LamC RNAi* flies but not in *LamB* RNAi flies. Multiple lines per map indicate multiple sequencing runs of biological replicates. DAR fold change is annotated for each comparison.

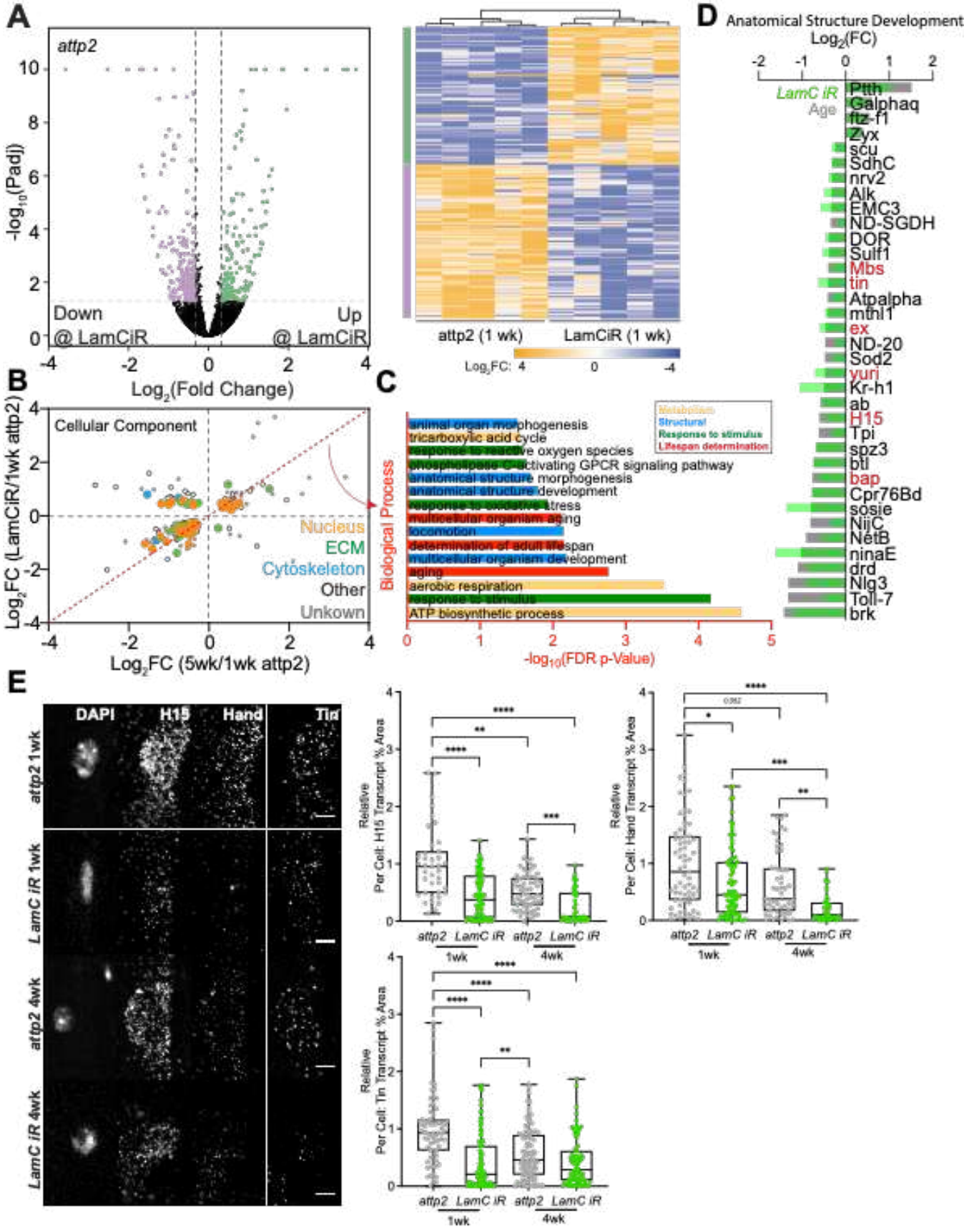
A
attp2
-log10(Padj)
Down @ LamCiR
Up @ LamCiR
Log2(Fold Change)
attp2 (1 wk)
LamCiR (1 wk)
Log2FC: 4 0 -4
B
Cellular Component
Log2FC (LamCiR/1wk attp2)
Log2FC (5wk/1wk attp2)
Nucleus
ECM
Cytoskeleton
Other
Unkown
C
Metabolism
Structural
Response to stimulus
Lifespan determination
Biological Process
animal organ morphogenesis
tricarboxylic acid cycle
response to reactive oxygen species
phospholipase C-activating GPCR signaling pathway
anatomical structure morphogenesis
anatomical structure development
response to oxidative stress
multicellular organism aging
locomotion
determination of adult lifespan
multicellular organism development
aging
aerobic respiration
response to stimulus
ATP biosynthetic process
-log10(FDR p-Value)
D
Anatomical Structure Development
Log2(FC)
LamC iR
Age
Pth
Galphaq
ftz-f1
Zyx
scu
SdhC
nrv2
Alk
EMC3
ND-SGDH
DOR
Sulf1
Mbs
tin
Atpalpha
mthl1
ex
ND-20
Sod2
yuri
Kr-h1
ab
H15
Tpi
spz3
btl
bap
Cpr76Bd
sosie
NijC
NetB
ninaE
drd
Nlg3
Toll-7
brk
E
DAPI
H15
Hand
Tin
attp2 1wk
LamC iR 1wk
attp2 4wk
LamC iR 4wk
Relative Per Cell: H15 Transcript % Area
Relative Per Cell: Hand Transcript % Area
Relative Per Cell: Tin Transcript % Area
attp2
LamC iR
1wk
4wk

1055

Figure 5: LamC Loss Transcriptionally Regulates Myogenic Transcription Factors. (A) Volcano plot and heat map of bulk RNA-seq from surgically dissected heart tubes from *LamC RNAi* flies compared to *attp2* control background flies at 1-week of age. 344 DEGs were assessed from cutoffs of -1.25 > FC > 1.25 and p-adj < 0.05 (dashed lines) from comparisons of 15 fly hearts in quadruplicate biological replicates; DEGs increasing and decreasing with *LamC* RNAi are shown in green and purple, respectfully. **(B)** Scatter plot is shown comparing fold changes from aging (1- and 5-weeks of age) and *LamC RNAi* compared to control background (*attp2*). Data was categorized based on which cellular component ontology term it most closely matches. Distance from the red dashed line of unity was used identify co-regulated genes whose **(C)** biological process ontology terms were annotated and ordered based on their false discovery rate p-value. **(D)** Genes within the anatomical structure term were plotted for their fold change for aging (gray) and *LamC RNAi* (green). Genes names in red represent myogenic transcription factors or muscle-specific structure proteins. **(E)** Representative images (left) of *in situ* hybridization chain reaction for transcription factors *H15*, *Hand,* and *tin,* co-stained with DAPI, for *LamC RNAi* and control *attp2* flies at 1- and 4-weeks of adulthood. A plot for each transcription factor is also shown (right) and quantifies the per cell percent area covered by each transcript. For *H15*, n = 39, 76, 64, and 45 cells for 1-week control, 1-week *LamC RNAi*, 4-week control, and 4-week *LamC RNAi*, respectively. For *Hand*, n = 71, 84, 52, and 43 cells for 1-week control, 1-week *LamC RNAi*, 4-week control, and 4-week *LamC RNAi*, respectively. For *tin*, n = 69, 101, 103, and 85 cells for 1-week control, 1-week *LamC RNAi*, 4-week control, and 4-week *LamC RNAi*, respectively. *p<0.05, **p<10^{-2}, ***p<10^{-3}, and ****p<10^{-4} by one-way ANOVA with Tukey multiple comparisons test.

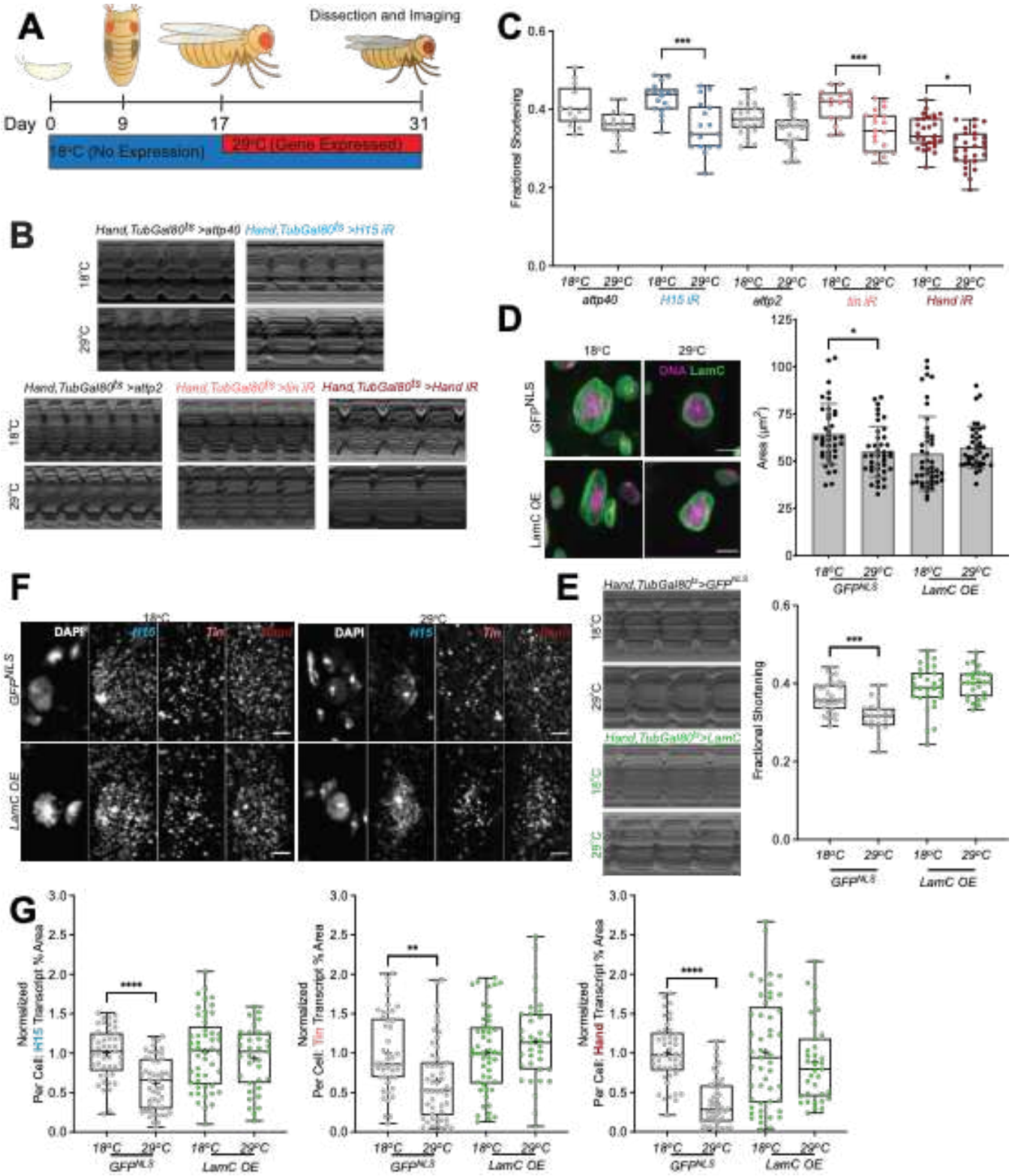

Figure 6: Myogenic Transcription Factors Diminish with Age and LamC Overexpression can Rescue Decreased Heart Function. (A) Schematic of temperature sensitive transgenic

expression where 29°C enables transgenic expression due to the denaturation of Gal4 transcription factor suppressor, $Gal80^{ts}$. **(B)** Representative kymographs of surgically exposed heart tubes at 18°C and 29°C for *attp2* and *attp40* controls (black), *tin RNAi* (pink), *Hand RNAi* (brown), and *H15 RNAi* (blue) and **(C)** quantification of their respective fractional shortenings at indicated temperatures are shown. n = 13, 15, 18, 15, 26, 27, 16, 19, 29, 27, 29, and 21 (heart tubes/transgene/ temperature; left to right). **(D)** Representative images (left) of nuclei from flies at 18°C and 29°C expressing a generic GFP^{NLS} transgene or an overexpression of *LamC* (*LamC* OE). To the right is a plot of projected nuclear area as a function of temperature and transgene expression. n = 39, 40, 46, and 41 nuclei (left to right). **(E)** Representative kymographs (left) of surgically exposed heart tubes for *LamC* OE (green) and generic GFP^{NLS} transgene (black) at 18°C and 29°C. Fractional shortening (right) is plotted for the same conditions and transgenes. n = 37, 20, 30, and 26 heart tubes. **(F)** For GFP^{NLS} and *LamC* OE at 18°C and 29°C, representative images for *in situ* hybridization chain reaction are shown for *tin* (pink), *Hand* (brown), and *H15* (blue) transcripts. **(G)** A plot for each transcription factor is shown and quantifies the per cell, percentage area for each transcript. *$p<0.05$, **$p<10^{-2}$, ***$p<10^{-3}$, and ****$p<10^{-4}$ by one-way ANOVA with Kruskal-Wallis test and Dunn's comparisons test.

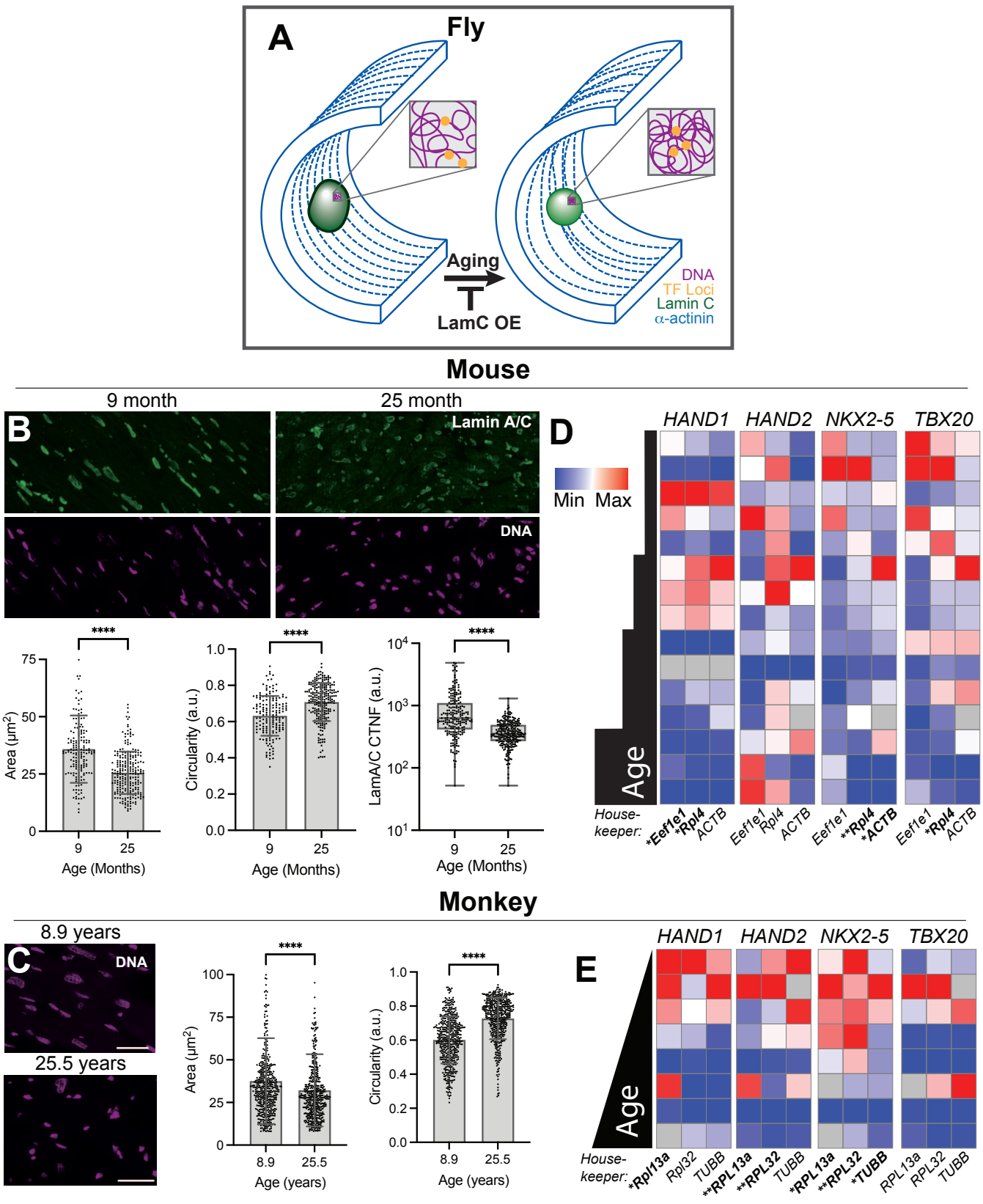

Figure 7: Nuclear remodeling induces adult-onset transcription factor loss, a process

conserved in Mice and Non-human Primates. (A) Schematic depicting how age-associated, cardiac-specific reduction of nuclear lamins reduces nuclear volume and chromatin accessibility, especially for myogenic transcription factors. With less muscle transcription from key cardiac loci, sarcomeres become disordered with age and heart function is reduced. Lamin overexpression can overcome age-associate reduction and preserve function. **(B)** Immunofluorescent staining of mouse heart sections at 9 and 29 months of age with anti-LamA/C (green) and DAPI (magenta). Below shows plots of projected nuclear area and circularity with respective ages. n = 3 biological replicates and 3 technical replicates. **(C)** Immunofluorescent staining of monkey left ventricle sections at 8.9 and 25.5 years of age with anti-LamA/C (green) and DAPI (magenta). Below shows plots of projected nuclear area and circularity with respective ages. n = 3 biological replicates and 3 technical replicates. qPCR results are plotted for **(D)** mouse and **(E)** rhesus macaque for the myogenic transcription factors Hand 1, Hand 2, Nkx2-5, and TBX20 as normalized by housekeepers Eef1e1, Rpl4, and ACTB for mouse and Rpl13a, Rpl20, and TUBB2 for macaque. Data were normalized to maximum and minimum expression within each gene and housekeeper for heatmap. *$p<0.05$, **$p<10^{-2}$, ***$p<10^{-3}$, and ****$p<10^{-4}$ by unpaired t-test (B, circularity) and with Welch's correction in (B, nuclear area). Significance in (C) and (E) indicate deviation from 0 for simple linear regression.

Supplementary Files

This is a list of supplementary files associated with this preprint. Click to download.

- ManuscriptSupplementalNatureAging.pdf